Facilitating interstellar searches for simple amino alcohols with accurate rest frequencies into the millimeter-wave regime: Alaninol, valinol, and leucinol

BENJAMIN E. ARENAS [iD],[1,2] MARIYAM FATIMA [iD],[1,2] CRISTÓBAL PÉREZ [iD],[1,2] SOPHIE FISCHER,[1,3]
AMANDA L. STEBER [iD],[1,2] AND MELANIE SCHNELL [iD][1,2]

[1] Deutsches Elektronen-Synchrotron (DESY), Notkestraße 85, 22607 Hamburg, Germany
[2] Institut für Physikalische Chemie, Christian-Albrechts-Universität zu Kiel, Max-Eyth-Straße 1, 24118 Kiel, Germany
[3] Current address: Department of Informatics, University of Bergen, Thormøhlensgate 55, N-5008 Bergen, Norway

ABSTRACT

The detection of larger complex organic molecules, such as molecules consisting of several functional groups or those which show conformational flexibility, in the interstellar medium could lead to insights into the availability of biomolecules in space. We present the rotational spectroscopic study of three amino alcohols: alaninol, valinol, and leucinol. The spectra were recorded over the 2-110 GHz region, which included the utilisation of a newly developed instrument operating between 18-26 GHz. We report accurately determined line lists, rotational constants, centrifugal distortion constants, and nuclear quadrupole coupling constants for two conformers of alaninol, four conformers of valinol, and three conformers of leucinol, as well as for several singly substituted heavy-atom isotopologues, which also provide structural insights. Further, a number of spectra of vibrationally excited states were assigned, and the associated motions were revealed with anharmonic frequency calculations. Accurate predictions of rotational transitions into the millimeter-wave regime for all species were made, facilitating searches for these complex molecules by observational facilities such as ALMA. Their detection would establish a new family of interstellar molecules.

Keywords: astrochemistry — molecular spectroscopy — high-resolution spectroscopy — spectral line lists — interstellar medium — interstellar molecules

1. INTRODUCTION

Over 200 molecules (Müller et al. 2005; Endres et al. 2016; McGuire 2018) have already been detected in the interstellar medium (ISM)[1], and many of these molecules contain biologically-relevant functional groups that could become incorporated into larger biomolecular motifs. Examples include alcohols and diols (important for their -OH groups), simple cyano-containing molecules (thought to be important for the incorporation of nitrogen into complex molecules), and even the simple sugar glycolaldehyde (Hollis et al. 2000).

As a consequence of increasingly sensitive observational facilities, larger and more complex molecules are becoming targets for interstellar searches. For example, recently, branched, chiral, and aromatic molecules were identified in space. The amino alcohols are interesting targets for astronomical detections. The family of molecules contain two functional groups - the amino group and the alcohol group - both of which have already been identified in interstellar space. The novel identification of this family of compounds in the ISM is the natural, next step in molecular complexity. Molecules that show conformational flexibility, which is another degree of complexity that can be exhibited by larger

Corresponding author: Amanda L. Steber
amanda.steber@desy.de

Corresponding author: Melanie Schnell
melanie.schnell@desy.de

[1] See the Cologne Database for Molecular Spectroscopy (CDMS), http://www.ph1.uni-koeln.de/cdms/.

and branched molecules, are also important targets, and the amino alcohols, particularly the larger molecules, are such examples.

This study aims at providing a complete rotational spectroscopic characterisation for these molecules to enable their detection in interstellar space using the modern, high sensitivity telescopes available. With 3, 5, and 6 carbon atoms (or 5, 7, and 8 heavy atoms), these molecules are in the typical range of the new species that have been detected in recent years. **While their potential formation routes, either in the gas phase or on ice grains, might still be an open question, the observation of other molecules containing amino or hydroxyl groups or even both (for example, hydroxylamine) makes a search for these amino alcohols promising.**

We also aim at unravelling the conformational flexibility of these molecules. It is important for this attribute to be well explored and that accurate line lists for the energetically relevant conformers exist. The reasons for this are two-fold. Firstly, the relative energies of the conformers can be considered, which can focus searches to the lower energy conformers which are more likely to be present, depending on the temperature of the environment. Secondly, accurate column densities of conformationally flexible molecules can be better achieved when all energetically available conformers are considered. The column density of the molecule is then based on the presence of multiple conformers, rather than on the presence of one variant, for example, as described in Zuckerman et al. (1975) and Pearson et al. (1997) for ethanol.

There have been several previous studies on smaller amino alcohols for the purposes of supporting astronomical detections. For example, the millimeter wavelength spectroscopy experiments of 2-aminomethanol (Widicus et al. 2003), which determined rotational and centrifugal distortion constants for the ground state and a number of vibrationally excited states, extended previous work on the molecule (Penn & Curl 1971; Kaushik & Woods 1982). 2-Aminomethanol, also known as glycinol, is the simplest amino alcohol that is related to the proteinogenic α-amino acid glycine. Several larger amino alcohols have also been examined by rotational spectroscopy, including serinol, which was studied as a model system for the lipid sphingosine (Loru et al. 2016). Another extensive survey along these lines involved a group of molecules, consisting of D-allothreoninol, 2-amino-1,3-propanediol, and 1,3-diamino-2-propanol, being studied to analyse the competition between cyclic and chain hydrogen-bonded motifs (Zhang et al. 2016).

In a previous structural analysis of an amino alcohol that is analogous to the proteinogenic α-amino acid alanine, Ellingsen et al. (1978) reported a microwave spectroscopy investigation of alaninol with transitions between 18.6-39.7 GHz. Their experimental analysis revealed the two lowest-energy conformers, each with an intra-molecular hydrogen bond. They also observed the pure rotational spectra of vibrationally excited states, four for Rotamer I and two for Rotamer II, which can facilitate their radioastronomical detection. The work was followed by a matrix-isolation infrared and Raman spectroscopy study from Fausto et al. (2000), where three further conformations were identified.

Amino alcohols and amino acids are appealing targets for interstellar searches, as important questions in astrochemistry are whether an essential amino acid exists in the gas phase in the ISM and, if so, what are its possible formation pathways. Searches for amino acids in the ISM are not new, with the first reported observation of interstellar glycine in 2003 (Kuan et al. 2003). Despite this observation eventually being disconfirmed (Snyder et al. 2005; Jones et al. 2007; Cunningham et al. 2007), amino acids are still of paramount interest in interstellar (bio-)chemistry. The amino alcohols are chemically related to amino acids and essentially represent a reduced state of the corresponding acid; that is, the acid can be produced from the alcohol via an oxidation process. In the gas phase and under radiative conditions, one could speculate that the alcohol species might be more stable than the carboxylic acid counterparts, which are likely to lose CO_2.

Several small proteinogenic α-amino acids have been characterised by microwave spectroscopy, including alanine, valine, and leucine (Blanco et al. 2004; Lesarri et al. 2004; Cocinero et al. 2007). Each work deduced that the gas-phase structure of the lowest energy conformers of the amino acids contain a bifurcated hydrogen bond between the hydrogen atom of the amino group and the carboxyl oxygen. The portfolio of work also provides the rotational constants required to search for the respective amino acids in the ISM. This has been noteworthy recently because of the detection of glycine, the simplest amino acid, in the coma of the comet 67P/Churyumov-Gerasimenko (Altwegg et al. 2016).

We present here a study of three potential proteinogenic α-amino acid precursors – alaninol (2-amino-1-propanol), valinol (2-amino-3-methyl-1-butanol), and leucinol (2-amino-4-methyl-1-pentanol) – with high-resolution, broadband rotational spectroscopy, also known as molecular rotational resonance spectroscopy. Additionally, we link this to our work on isoleucinol (2-amino-3-methyl-1-pentanol; Fatima et al. (2020)). The rotational spectra of these molecules are investigated across various bands of the 2-110 GHz region to identify and assign vibronic ground state conformers, singly substituted heavy-atom isotopologues, and vibrationally excited states.

These assignments will facilitate searches for these COMs, which are chemical relatives of amino acids, in the ISM by providing rotational constants and line lists, which are essential for their astronomical detections. Their presence would signify the observation of a new class of molecules not detected in the ISM before, and the successful detection of these amino alcohols could act as a signpost towards regions of the ISM where their amino acid analogues are more likely to be observed.

2. EXPERIMENTAL DETAILS

The rotational spectra of alaninol, valinol, and leucinol were recorded with our three chirped-pulse Fourier transform rotational spectrometers. The low-energy conformers were first identified using a supersonic expansion molecular beam on the Hamburg COMPACT spectrometer, between 2 - 8 GHz (Schmitz et al. 2012; Pérez et al. 2016) and 8 - 18 GHz (Fatima et al. 2020), and a newly built 18-26 GHz spectrometer (Fatima et al. 2020). The experiments in the millimeter-wave (mmw) regime were carried out on our W-band (75-110 GHz) spectrometer (Arenas et al. 2017) at room temperature in a slow flow cell configuration. The spectrometers are summarised here for reference, with individual details for each spectrometer in the following paragraphs. Extensive descriptions of the apparatuses can be found in the corresponding publications. In short, all three spectrometers are chirped-pulse instruments that use an arbitrary waveform generator (AWG) to produce excitation pulses. These excitation pulses are transmitted into a vacuum chamber, where, when a frequency of the chirped excitation pulse is resonant with a molecular rotational transition, a macroscopic polarisation is induced. The resulting free induction decay (FID) of the gaseous sample is collected and fast Fourier transformed into the frequency domain. The number of co-added FIDs collected within each frequency range per molecule varied between 0.5 and 5.6 million, and an exact breakdown is given in Table A1. The samples were obtained from Alfa Aesar (L-alaninol, 98 % purity), Biozol (L-valinol, 98 % purity), and Fisher Scientific (L-leucinol, 98 % purity) and were used without further purification. The samples were heated to the following temperatures during the experiments **in order to increase their vapour pressures**: 80 °C for alaninol, 30 °C for valinol, and 125 °C for leucinol.

In the Hamburg COMPACT spectrometer, the excitation chirps cover the 2-18 GHz range in two separate arrangements. Before transmission into the chamber, the 2-8 GHz excitation pulses are amplified by a 300 W travelling wave tube amplifier (Schmitz et al. 2012; Pérez et al. 2016). For the 8-18 GHz region, a 50 W solid state amplifier is used to amplify the pulses, and to optimise the power per GHz in this range, the experiment is sub-divided into three different frequency regions - 8-13, 13-15.5, and 15.5-18 GHz (Fatima et al. 2020). The excitation chirps were 4 μs (2-8 GHz) and 2 μs long (8-18 GHz), and the FIDs were recorded for 40 μs (2-8 GHz) or 20 μs (8-18 GHz). The instrument has a resolution of 25 kHz for the 2-8 GHz band and 50 kHz for the 8-18 GHz band. The samples were placed in a heatable reservoir nozzle (Parker Series 9 nozzle), and the molecular vapour was supersonically expanded into the vacuum chamber with 3 bar of neon as the backing gas, **which results in a sample rotational temperature of approximately 3 K.**

The newly designed 18-26 GHz spectrometer combines the segmented approach and the multi-train method. The segmented approach involves splitting the bandwidth into smaller segments, in this case the segments are 800 MHz wide, and the spectrum across the whole bandwidth is obtained by stitching the segments together (Neill et al. 2013). The multi-train method involves utilising multiple pulse trains per molecular pulse, which increases the effective repetition rate of the experiment (Fatima et al. 2020). The excitation pulses in the 3-7 GHz range, which are 1.5 μs in duration, are created by an AWG. The pulses are then frequency up-converted to 18-26 GHz with a number of mixing and doubling stages. The FIDs for each segment were collected, down-converted to 400-1200 MHz, and recorded for 10 μs. Each segment was then corrected to its original frequency by the addition or subtraction of a local oscillator frequency, which was followed by segment concatenation, giving the spectrum across the whole band. The resulting resolution of the spectrometer is approximately 100 kHz. Full details of this instrument appear in Fatima et al. (2020). The sample was placed in a similar heatable reservoir nozzle as in the COMPACT. Neon, with a backing pressure of 1 bar, was used as the carrier gas.

The commercial W-band spectrometer from BrightSpec, Inc. operates in the frequency range 75-110 GHz, and it also uses the segmented approach (Arenas et al. 2017; Neill et al. 2013). The AWG produces excitation pulses initially in the range 1.6-2.3 GHz, which are then frequency up-converted and multiplied through a series of mixing stages and an active multiplier chain (x6). The instrument's High Dynamic Range mode (Arenas et al. 2017) was used to collect the spectra shown here. Each segment was 30 MHz wide, the pulse duration was 500 ns, and the FID was recorded for 4 μs. The spectrometer has a resolution of approximately 550 kHz. The room-temperature **(approximately 300**
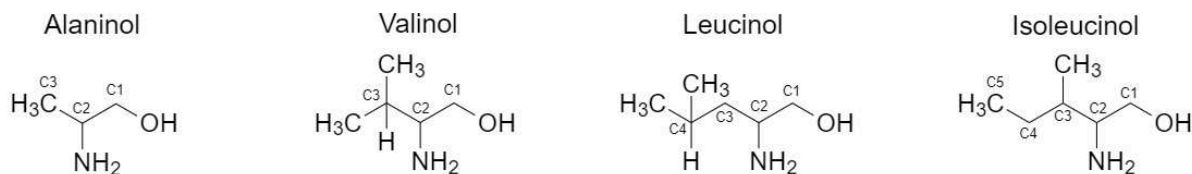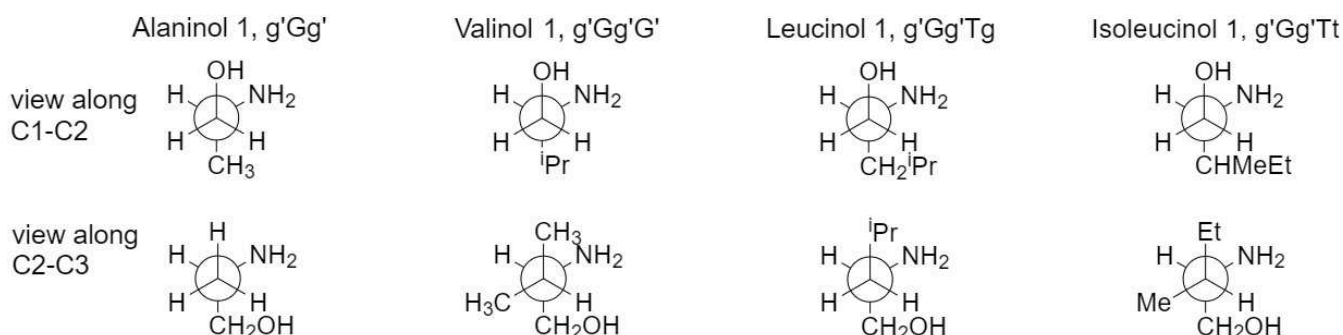
Figure 1. (a) The Lewis structures of the three amino alcohols alaninol, valinol, and leucinol. The structure of isoleucinol, the rotational spectroscopy study of which we report in a sister publication (Fatima et al. 2020), is shown for completeness. (b) The Newman projections of the lowest energy conformers; see text for discussion.

K), high-frequency experiments were performed under slow flow cell conditions, with the sample being pre-treated in a freeze-pump-thaw manner to remove any air from the external reservoir. The samples were then heated **to be aforementioned temperatures to increase their vapour pressures**, vapour was allowed to flow into the chamber without a backing gas, and a pressure of 10 μbar was maintained in the chamber for all samples.

3. THEORETICAL WORK

All three molecules studied here are flexible; rotations around their C-C single bonds (see structures in Figure 1(a)) can result in a number of different possible conformations. Conformational searches were conducted for each molecule in the same manner. First, automated semi-empirical conformational searches were done on the SPARTAN program using the Austin Model 1 (AM1) method, the Parameterization Method 3 (PM3), and the Parameterization Method 6 (PM6) (Spartan 14 www.wavefun.com). After sorting through the structures to remove duplicates, each returned structure was re-optimised with the B3LYP-D3(BJ) exchange-correlation functional (Becke, three-parameter, Lee-Yang-Parr), including Grimme's empirical dispersion correction with Becke Johnson damping and the def2-TZVP basis set using the Gaussian 09 program package (Frisch et al. 2009). Structures from all three methods that were considered to be energetically accessible to us in our experiments were re-optimised at the B3LYP-D3(BJ)/aug-cc-pVTZ level of theory. The energetic considerations followed those made in Domingos et al. (2016) and focus the list of potential conformers to those which have energies within 6 kJ mol^{-1} of the lowest energy structure. The number of conformers of each molecule from each method were as follows: alaninol – two conformers from AM1, three conformers from PM3, two conformers from PM6; valinol - four conformers from AM1, four conformers from PM3, three conformers from PM6; leucinol - two conformers from AM1, five conformers from PM3, one conformer from PM6. This resulted in three distinct conformers for alaninol, four distinct conformers for valinol, and five distinct conformers for leucinol, all of which were searched for in the experimental spectra. The automated conformational searches were supplemented with manual dihedral angle scans along the carbon backbones of the molecules. The scans were performed at the B3LYP/6-311G++ level of theory, and each resulting minimum was re-optimised at the B3LYP/aug-cc-pVTZ level of theory. The results from both methods produced the same final list of conformers. The collated list of final conformers was used to aid in spectral assignment. Additionally, for alaninol, we were guided by the conformational landscape reported by Fausto et al. (2000) in their matrix-isolation infra-red study. In order to maintain consistency, the naming

scheme of the conformers we used was based on the work by Ellingsen et al. (1978) and Fausto et al. (2000), and it is extended here to include the longer carbon chains of leucinol and valinol. The details are included in Appendix B.

Anharmonic frequency calculations, at the B3LYP-D3(BJ)/aug-cc-pVTZ level of theory, were performed for each assigned conformer in order to obtain theoretical rotational constants for their vibrational states. To aid with the assignments, the calculated rotational constants for the vibrational states were shifted by the difference observed between the experimental and calculated rotational constants for the respective ground state conformer. The anharmonic frequency calculations also provided theoretical quartic distortion constants to aid in the assignment of the ground state conformers in the W-band datasets.

4. ANALYSIS

The amino alcohols studied here are all asymmetric tops, where $A \neq B \neq C$. The theoretical and experimental values for Ray's asymmetry parameter, κ, for each conformer are given in Tables 1-3, where

$$\kappa = \frac{2B - A - C}{A - C}. \tag{1}$$

Generally, the values of κ range from -1 to 1, where these two limits are indicative of symmetric prolate and symmetric oblate tops, respectively. All of the conformers are asymmetric, near-prolate tops, with the theoretical κ values ranging from -0.99 to -0.48. They were thus fit to a Watson's A-reduction Hamiltonian in the I^r representation. Spectral analysis was carried out using the PGOPHER program (Western 2017) and the AABS program package (Kisiel et al. 2005; Kisiel 2015). The final fits were obtained from Pickett's suite of programs (SPFIT/SPCAT) (Pickett 1991).

The low frequency datasets, up to 26 GHz, exhibited hyperfine splitting due to the nuclear electric quadrupole moment of the nitrogen nucleus. This hyperfine splitting was only relevant for these datasets, and not for the W-band spectra, as the splitting collapses for transitions with high rotational quantum number, J. In order to obtain a fit encompassing all of the measured transitions, a global fit was performed whereby the rotational constants and the quartic centrifugal distortion constants were fit to all assigned lines, and the nitrogen nuclear quadrupole coupling constants were fit only to those lines which exhibited the hyperfine splitting. That is, any transition exhibiting hyperfine splitting was labelled with the relevant F-state labels, and those which did not exhibit the splitting were assigned to a pure rotational Hamiltonian. Further details on this can be found in Giuliano et al. (2019), where the same procedure in the analysis of the rotational spectrum of imidazole was used.

The substitution structures of some of the amino alcohols were determinable because singly-substituted isotopologues were observed in natural abundance. This analysis was performed using the KRA program package, and further structural analysis, such as the determination of dihedral angles, was performed with the EVAL program package (Kisiel et al. 2005; Kisiel 2015).

5. RESULTS AND DISCUSSIONS

The spectroscopic parameters for the observed ground state conformers of alaninol ($g'Gg'$ and $gG'g$), valinol ($g'Gg'G'$, $g'Gg'G$, $g'Gg'T$, and $gG'gG'$), and leucinol ($g'Gg'Tg$, $g'Gg'Gg'$, and $gG'gTg'$) are presented in Tables 1-3, respectively. In these tables, the experimentally determined constants are listed alongside those obtained from theory (as described above). The theoretical rotational constants agree with the experimental rotational constants within a 0.4 % difference for alaninol, a 0.6 % difference for valinol, and a 0.7 % difference for leucinol. A comparison to the previously published rotational constants of alaninol (Ellingsen et al. 1978) is also presented in Table 1. The improvement of the microwave root mean square (σ) between the current analysis of alaninol and that performed by Ellingsen et al. (1978) highlights the experimental frequency accuracy available from modern high-resolution rotational spectroscopy. The fits for alaninol 1, $g'Gg'$, alaninol 2, $gG'g$, valinol 1, $g'Gg'G'$, and valinol 2, $g'Gg'G$, are the result of combining data from the ranges 2-26 and 75-110 GHz. Valinol 3, $g'Gg'T$, and valinol 4, $gG'gG'$, were not assigned in the W-band spectrum, likely due to a combination of low signal-to-noise of these higher energy conformers and difficulties in pinpointing transitions in the confusion-limited spectrum.

Despite extensive efforts, including performing frequency calculations at various levels of theories and basis sets to obtain theoretical rotational and distortion constants, none of the vibronic ground states nor vibrationally excited states of leucinol could be assigned in the room-temperature W-band spectrum. Extrapolation of the rotational constants determined from the low frequency data (2-26 GHz) into the 75-110 GHz region predicts nineteen R-branch transition sets (J=43 to J=61). But there are no identifiable transition features or patterns in the **high-frequency** spectrum,

indicating that the measured species **in the W-band experiment** was not leucinol, but perhaps a degradation product.

For all systems, the spectra recorded with the COMPACT and the 18-26 GHz spectrometers showed hyperfine splitting, caused by the interaction of the ^{14}N I=1 spin with the electric field gradient. This is shown clearly in Figure 2, where a section of the rotational spectrum of alaninol is plotted against the simulated spectrum of the fitted rotational constants for the lowest energy conformer, $g'Gg'$. The hyperfine splitting generally spans 2-3 MHz for alaninol 1, $g'Gg'$, and this holds true for the other amino alcohol conformers. Analysis of this effect has allowed us to determine the nitrogen nuclear quadrupole coupling constants χ_{aa} and χ_{bb}-χ_{cc} for all ground state conformers and a number of isotopologues. Comparison of these experimental constants to those computed from theory provides a further confirmation of the structure designated to each assignment. These constants are of particular importance for interstellar searches, as the observation of nuclear hyperfine splitting can act as a further validation mechanism for interstellar detections (Loomis et al. 2013; McGuire et al. 2018).

In addition to the low-energy conformers listed above, we also observed the rotational spectra of a number of isotopologues in natural abundance in the 2-26 GHz datasets. The application of Kraitchman's equations (Kraitchman 1953) allowed us to experimentally determine the position of each isotopically substituted atom with respect to the molecule's centre of mass. A comparison of the experimentally determined substitution structures in the gas phase and the quantum-chemically optimised structures is presented in Figure 3 for those that were observed. The partially transparent molecular structure is the optimised structure at the B3LYP-D3(BJ)/aug-cc-pVTZ level of theory, and the coloured spheres are the experimentally determined atom positions. As shown, the theoretical structures match the experimental structures. Isotopologues were observed for the following conformers: ^{13}C, ^{15}N, and ^{18}O for alaninol 1 ($g'Gg'$) and valinol 1 ($g'Gg'G'$); ^{13}C and ^{15}N for alaninol 2 ($gG'g$), valinol 2 ($g'Gg'G$), and leucinol 1 ($g'Gg'Tg$). A full account of the rotational constants for the isotopologues observed is reported in Tables C1-C5. The analysis of the isotopologues allowed us to unambiguously determine the experimental backbones of the alaninol conformers, the two lowest energy conformers of valinol, and the lowest energy conformer of leucinol. Aside from the structural analysis that can be developed from this information, which follows below, this information can be useful to astronomers in the future for searches for these species in the ISM. Searches of this nature would rely on any parent-species conformer being detected in sufficient abundance, and the likeliness of detection would be increased with the continuously improving sensitivities of observational facilities. Heavy-atom isotopologue detections, despite currently being relatively rare in comparison to detections of main-isotopologue species, could in the future provide information on isotopic fractionation and reveal reaction pathways in specific regions (Furuya et al. 2011).

Table 1. The experimental and theoretical rotational constants for the observed ground state conformers of alaninol. The experimental values for both conformers are the result of global fits of the data in the regions 2-18, 18-26, and 75-110 GHz. The theoretical parameters were obtained at the B3LYP-D3(BJ)/aug-cc-pVTZ level of theory. The rotational constants reported by Ellingsen et al. (1978) are included for comparison.

	Conformer 1, $g'Gg'$			Conformer 2, $gG'g$		
	This work	Theory	Ellingsen et al. (1978)	This work	Theory	Ellingsen et al. (1978)
A / MHz	7948.48588(88)	7972.7	7948.403(77)	6461.60804(69)	6487.9	6461.620(32)
B / MHz	3640.57864(28)	3645.7	3640.570(11)	4144.43502(37)	4134.6	4144.442(30)
C / MHz	2747.73691(20)	2749.7	2747.727(11)	3336.16546(34)	3328.9	3336.163(30)
Δ_J / kHz	0.72345(80)	0.7	0.51(18)	1.6343(17)	1.6	1.65(69)
Δ_{JK} / kHz	3.4438(58)	3.4	3.84(63)	4.940(10)	5.1	6.35(15)
Δ_K / kHz	2.024(87)	2.5	1.5(3.2)	−3.701(48)	−3.7	−7.02(40)
δ_J / kHz	0.17391(29)	0.2	0.163(24)	0.24994(53)	0.3	0.3420(94)
δ_K / kHz	2.321(13)	2.3	3.23(56)	1.115(16)	1.1	−0.034(117)
χ_{aa} / MHz	−3.6734(33)	−4.1		−0.7119(50)	−0.8	
χ_{bb}-χ_{cc} / MHz	−0.1108(68)	−0.18		4.0368(72)	4.4	
μ_a, μ_b, μ_c / D		3.1, 0.5, 0.4	3.03(1), 0.54(3), 0.57(19)		2.5, 0.91.3	2.19(3), 1.46(8), 1.172(3)
κ	−0.66	−0.66	−0.66	−0.48	−0.49	−0.48
No. of lines	258		39	251		36
σ / kHz	13.7		112	18.2		75.8
J_{max}, K_{max}	18, 17			15, 14		

Table 2. The experimental and theoretical rotational constants for the observed ground state conformers of valinol. The experimental values for conformers 1, $g'Gg'G'$, and 2, $g'Gg'G$, are the result of global fits of the data in the regions 2-18, 18-26, and 75-110 GHz. The experimental values for conformers 3, $g'Gg'T$, and 4, $gG'gG'$, are the result of fits of the data from 2-26 GHz. The theoretical parameters were obtained at the B3LYP-D3(BJ)/aug-cc-pVTZ level of theory. Values contained within square brackets were kept fixed to the theoretical values.

| | Conformer 1, $g'Gg'G'$ | | Conformer 2, $g'Gg'G$ | | Conformer 3, $g'Gg'T$ | | Conformer 4, $gG'gG'$ | |
	This work	Theory	This work	Theory	This work	Theory	This work	Theory
A / MHz	4023.53359(37)	4036.8	4236.8058(15)	4249.7	3629.76830(45)	3651.3	3411.43927(47)	3432.0
B / MHz	1701.31802(14)	1702.8	1546.61067(26)	1549.3	1691.76050(54)	1694.5	2011.33242(29)	1998.1
C / MHz	1284.21089(12)	1284.2	1414.10206(23)	1413.1	1470.41499(43)	1466.5	1486.51765(23)	1483.0
Δ_J / kHz	0.108023(72)	0.1	0.22047(15)	0.2	0.2656(49)	0.3	0.3400(43)	0.4
Δ_{JK} / kHz	0.18277(36)	0.2	0.12889(98)	0.1			0.242(24)	−0.01
Δ_K / kHz	0.724(22)	0.9	[1.039662972]	1.0				
δ_J / kHz	0.026377(33)	0.03	0.043245(77)	0.04	0.0362(29)	0.04	0.1216(23)	0.1
δ_K / kHz	0.2496(16)	0.3	4.825(13)	4.9	3.05(15)	1.8		
χ_{aa} / MHz	−4.1801(33)	−4.6	−3.9918(49)	−4.5	−4.2541(36)	−4.7	0.2715(30)	0.5
χ_{bb}-χ_{cc} / MHz	0.6928(64)	0.6	−0.6612(48)	−0.6	0.7028(76)	0.5	4.7808(52)	5.3
μ_a, μ_b, μ_c / D		3.0, 1.2, 0.7		3.1, 0.3, 0.7		2.8, 1.7, 0.4		1.5, 1.7, 1.5
κ	−0.70	−0.70	−0.91	−0.90	−0.79	−0.79	−0.45	−0.47
No. of lines	569		172		184		258	
σ / kHz	20.1		15.7		12		11.8	
J_{max}, K_{max}	42, 42		36, 34		8, 8		8, 8	

Table 3. The experimental and theoretical rotational constants for the observed ground state conformers of leucinol. The experimental values for all three conformers are the result of fits of the data from 2-26 GHz. The theoretical parameters were obtained at the B3LYP-D3(BJ)/aug-cc-pVTZ level of theory.

| | Conformer 1, $g'Gg'Tg$ | | Conformer 2, $g'Gg'Gg'$ | | Conformer 3, $gG'gTg'$ | |
	This work	Theory	This work	Theory	This work	Theory
A / MHz	4047.45526(45)	4061.2	3338.49819(61)	3349.7	3438.92783(94)	3461.4
B / MHz	904.64031(11)	903.2	1017.18281(31)	1017.8	1044.55278(34)	1043.6
C / MHz	876.84190(12)	877.8	919.14552(29)	920.1	945.90732(33)	944.4
Δ_J / kHz	0.07316(22)	0.07	0.1125(14)	0.1	0.1065(13)	0.1
Δ_{JK} / kHz	0.4674(20)	0.4	0.1639(80)	0.2	$-0.0447(83)$	-0.07
Δ_K / kHz	1.198(29)	1.5	0.948(29)	1.1	1.307(72)	1.6
δ_J / kHz	0.01315(11)	0.01	0.0357(10)	0.03	0.02794(70)	0.03
δ_K / kHz	7.583(44)	9.0	1.272(74)	1.3	1.139(89)	1.1
χ_{aa} / MHz	$-3.8315(28)$	-4.2	$-3.309(8)$	-3.6	0.302(15)	0.4
χ_{bb}-χ_{cc} / MHz	$-1.0472(56)$	-1.0	$-0.1600(156)$	-0.4	$-1.1172(196)$	-1.1
μ_a, μ_b, μ_c / D		3.0, 0.2, 1.2		2.2, 2.2, 0.2		1.8, 2.3, 0.2
κ	-0.98	-0.98	-0.92	-0.92	-0.92	-0.93
No. of lines	419		238		180	
σ / kHz	12.8		17.2		18.3	
J_{max}, K_{max}	16, 16		13, 13		13, 13	

(a)

(b)
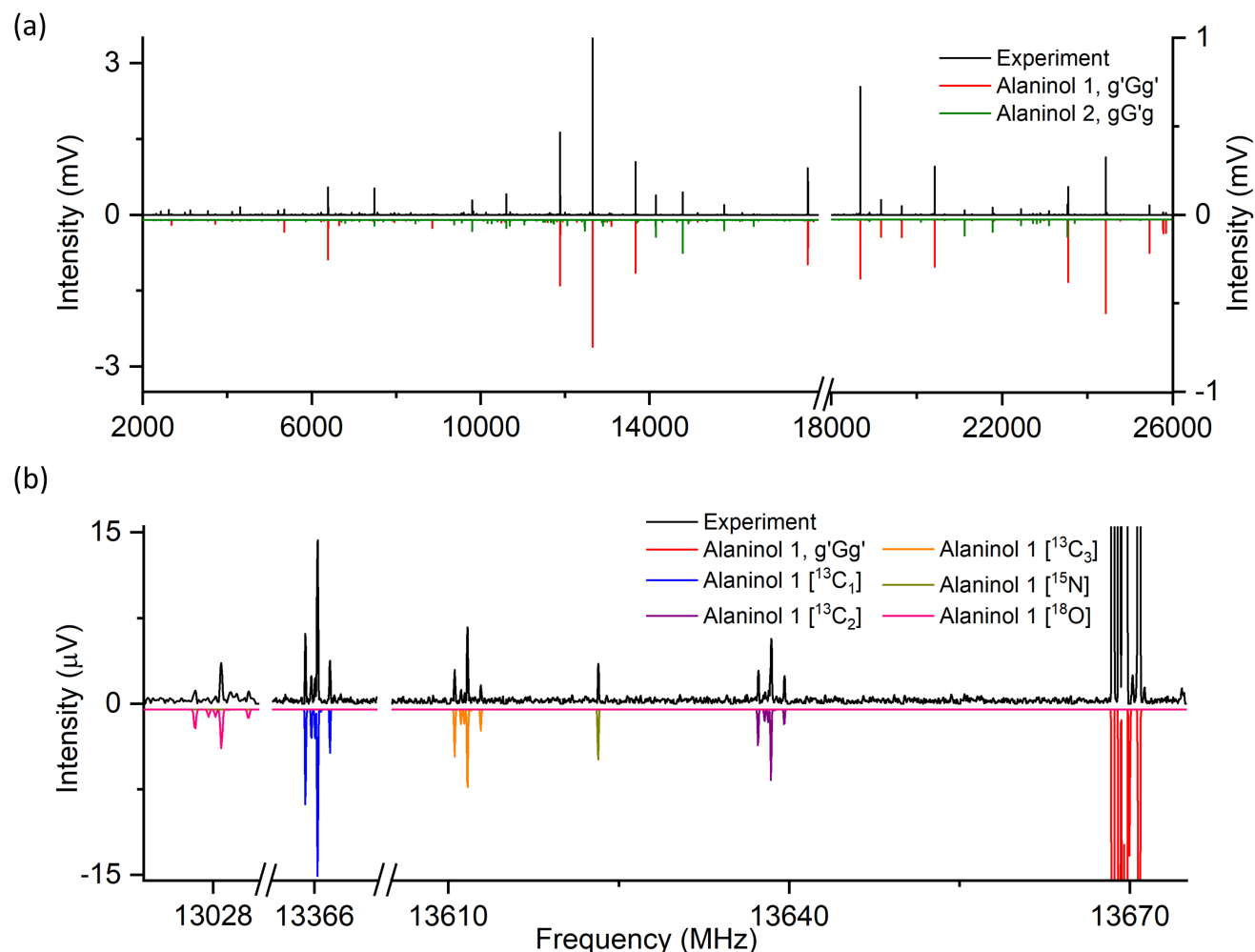
Figure 2. (a) The low-frequency (2-18 and 18-26 GHz) experimental datasets of the rotational spectrum of alaninol. The numbers of co-added FIDs, in millions, are 1.9, 1.1, 1.0, 1.4, and 2.6 in the 2-8, 8-13, 13-15.5, 15.5-18, and 18-26 GHz regions, respectively. Note the different intensity axes for the two different frequency ranges. (b) Zoom-ins to illustrate the assignments of the observed isotopologues for alaninol 1, $g'Gg'$ in the 13-15.5 GHz region. In both, the black trace is the experimental spectrum, and the coloured traces are simulated spectra based on the fitted rotational constants at 3 K, **which was the rotational temperature of the supersonic expansion.**

As can be seen in Figure 3, all of the lowest energy conformers of each amino alcohol have the same backbone in terms of the relative positions of the amino and the alcohol groups in the molecule. That is, they follow the structure of conformer 1 of alaninol, $g'Gg'$, where the conformer is dominated by the hydrogen-bond stabilisation between the –NH$_2$ and the –OH groups. Following the depiction in Figure 1(b), viewing the molecules' stabilised configuration along the C1-C2 bond clearly shows that the relatively large -X substituent is *anti* to the –OH group (-X = -Me for alaninol, -^{i}Pr for valinol, -CH$_2$ ^{i}Pr for leucinol, and -CHMeEt for isoleucinol). This was first discussed for alaninol by Ellingsen et al. (1978). If the molecule is viewed along the C2-C3 bond, the *anti* configuration for the –CH$_2$OH on C2 and the bulkiest substituent on C3 can also be noted. Where there is more than one non-hydrogen substituent on the C3 position, the second is positioned *anti* to the –NH$_2$ group. This is seen most clearly in isoleucinol, which was recently published and is included in Figure 1(b) for completeness, where the *anti* pairs along the C2-C3 bond are -CH$_2$OH/-Et and -NH$_2$/-Me. The differences between the molecules arise from the various additions to the carbon chain at the C3 position. One would expect that as more extended carbon groups are added to the C3 position, the number of low-energy conformers increases due to the higher number of C-C single bonds around which bond rotations can occur. However, steric effects do play a role, and this can be seen by the fact that a number of 'expected' conformers
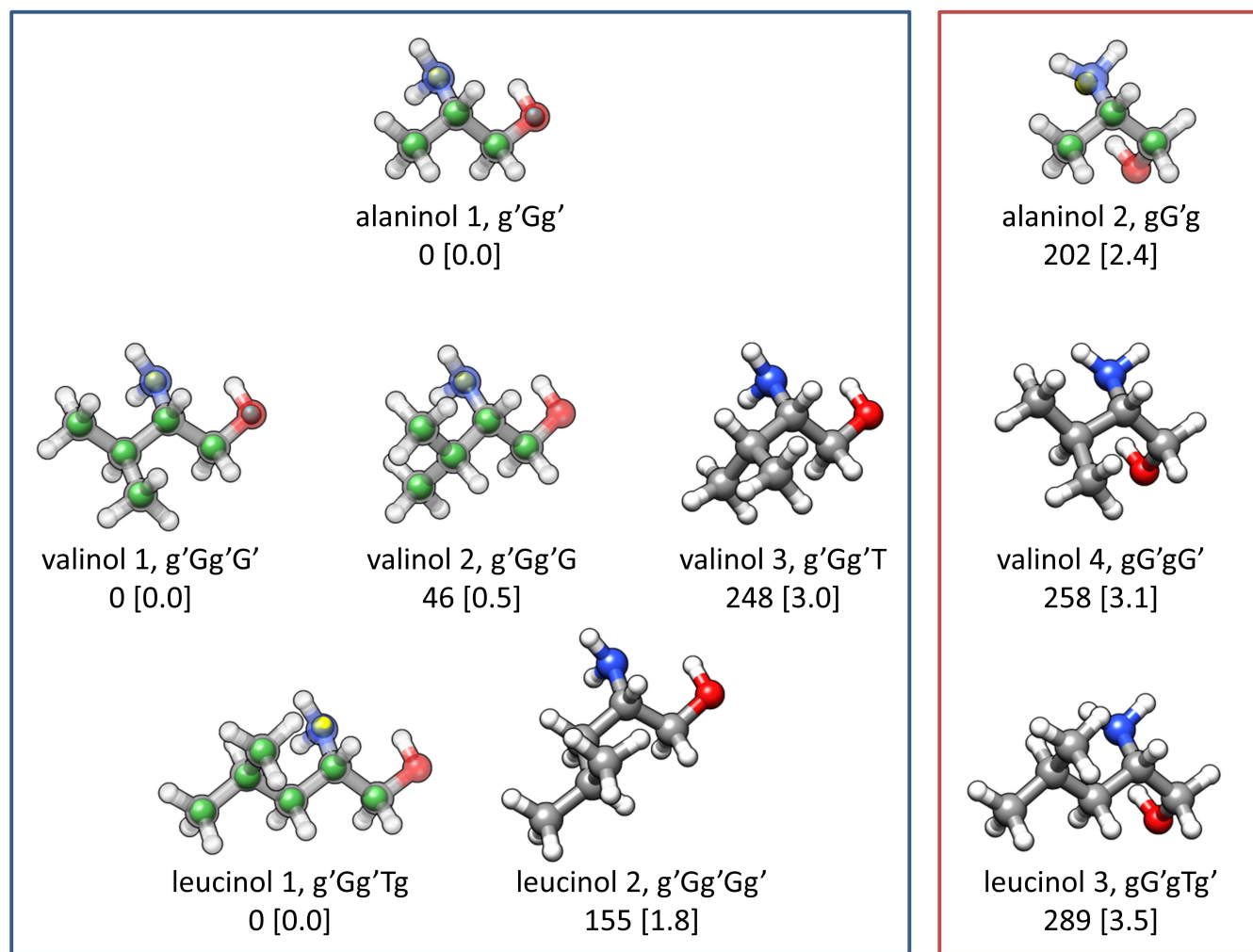
Figure 3. The structures of alaninol, valinol, and leucinol observed in our experiments. The structures shown were optimised at the B3LYP-D3(BJ)/aug-cc-pVTZ level of theory. The zero-point energy corrected energy values, in the format cm^{-1} [kJ mol^{-1}], are noted relative to the lowest energy conformer of that particular molecule. Where applicable, a comparison of the experimentally determined atom positions and the atom positions from the structure optimisation calculations are shown - the theoretical structures are in faded colour, and the solid spheres are the determined positions for carbon (green), nitrogen (yellow), and oxygen (cyan). The conformers are further sub-divided into the two hydrogen bond motifs named via the aBc dihedral angles - those within the blue box conform to the $g'Gg'$ dihedral angle template, those within the red box conform to the $gG'g$ dihedral angle template (see Appendix B for further details).

are not observed; for example, the hypothetical structure of leucinol 1, $g'Gg'Tg$ in which the C1-C2-C3-C4 dihedral angle is around -60° is not observed because of steric hindrance. Indeed, this hypothetical structure does not appear as a minimum in our conformational search, as it would likely interconvert to either leucinol 1, $g'Gg'Tg$, or leucinol 2, $g'Gg'Gg'$. Lesarri et al. (2004) have already noted steric effects as an important consideration in explaining 'missing' conformers. The structures of the amino alcohols follow chemical intuition when considering the *anti* configurations of the bulky substituents, but as already mentioned, steric effects should be considered as an important factor in determining if a structure will be observable in a supersonic expansion.

The studies on the rotational spectra of the relevant amino acids (Blanco et al. 2004; Lesarri et al. 2004; Cocinero et al. 2007) allow us to compare the structural motifs with the amino alcohol structures observed here. The lowest energy structures of all the observed amino acids in the gas phase (Conformer I in the relevant publications) contain a bifurcated hydrogen bond between the amino group and the oxygen of the carbonyl group. With the lack of a carbonyl group in the amino alcohol analogues, it is not surprising that the lowest energy conformers of the amino alcohols are not structurally similar to those of the amino acids. However, in all cases, the lowest energy amino

alcohol conformer resembles the motif of the next energetically favourable amino acid conformer observed; that is, alaninol 1, $g'Gg'$ resembles alanine IIa, valinol 1, $g'Gg'G'$ resembles valine IIa, and leucinol 1, $g'Gg'Tg$ resembles leucine IIb$_1$. In the same vein, we could show that the lowest energy conformer of isoleucinol, $g'Gg'Tt$, is structurally similar to isoleucine IIa$_1$ (Fatima et al. 2020). The major differences between the similar structures can be explained by the constitutional difference regarding the carbonyl group. The amino acids contain the carbonyl group, which itself adopts a planar structure due to the sp^2-hybridised carbon. In the study on alanine, Blanco et al. (2004) state that "the amino acid backbone is nonplanar", and this non-planarity is further emphasised in alaninol, wherein the sp^2-hybridised carbon is now an sp^3-hybridised carbon. This results in a tetrahedral arrangement around the C1 atom, and, thus, a non-planar arrangement of the backbone. The hydrogen bond between the amino group and the alcohol group (-N$\cdots$H-) increases from 1.96(1) $\mathring{A}$ in alanine IIa (Blanco et al. 2004) to 2.23 $\mathring{A}$ in alaninol 1, $g'Gg'$ (from our structure optimisation calculation), and the N-C2-C1-O dihedral angle, the dihedral angle effectively defining the backbone planarity, increases from -11.5(8)° in alanine IIa (Blanco et al. 2004) to 55.7(9)° in alaninol 1, $g'Gg'$. The dihedral angle in alaninol is the same as that reported previously, 54(2)° (Ellingsen et al. 1978), and it is in keeping with the dihedral angle from the theoretical structure at the B3LYP-D3(BJ)/aug-cc-pVTZ level of theory, which is 53.9°.

There is not as detailed an account of structural parameters in the studies of valine and leucine. This means that valinol and leucinol cannot be directly compared to their amino acid analogues in the same manner as alaninol can be compared to alanine. The experimental N-C2-C1-O dihedral angle for valinol 1, $g'Gg'G'$ is 50.5(7)°. This compares well with the dihedral angle in the optimised theoretical structure, which is 50.2°. Our study on isoleucinol revealed the same angle to be 50.9(8)° in isoleucinol 1, $g'Gg'Tt$, for which the theoretical value for the dihedral angle is 50.4° (Fatima et al. 2020). The full experimental substitution structure of leucinol 1, $g'Gg'Tg$ is not currently available, as the ^{18}O isotopologue was not observed in natural abundance. We expect, however, that the theoretical value (53.7°) will be an adequate estimation because of the agreement between experimental and theoretical values for the other amino alcohols in the series and the good agreement between experimental and theoretical rotational constants. All these values are in keeping with the dihedral angle in alaninol 1, $g'Gg'$, and they show a 3.8 % average deviation from the mean value. We speculate that these small deviations in the dihedral angles originate from the different groups on the C3 atoms of the molecules. In valinol and isoleucinol, the groups on the C3 atom could exhibit steric hindrance with the groups on the C2 atom, which would make the N-C2-C1-O dihedral angle deviate more from 60°. This effect is less pronounced for alaninol and leucinol, which both have fewer bulky groups on the C3 atom. This can be seen in the Newman projections in Figure 1(b) and follows from the earlier discussion about the projections. The dihedral angle N-C2-C1-O effectively defines the carbon backbone planarity in the amino alcohols studied, and the values reported here indicate non-planarity. Where data is available, an increase in the degree of non-planarity is seen when compared to the analogous amino acid.

The spectroscopic data for the vibrational states were accessible in the W-band experiments performed at room temperature. As stated previously, they could prove important if the ground state conformers are detected in warm regions of the ISM. The assignments of the vibrational states of alaninol conformer 1, $g'Gg'$ are shown in the zoom-ins in Figure 4. Figure D1 shows these motions alongside their energies with anharmonic corrections at the B3LYP-D3(BJ)/aug-cc-pVTZ level of theory. A short description of the fundamental modes follows: ν_{36} is the heavy atom torsion; ν_{35} is the rotation of the terminal methyl group; ν_{34} is a scissor motion of the carbon chain; ν_{33} is a motion in the –NH$_2$ group; ν_{32} is the –CH$_3$/-NH$_2$ scissor; ν_{31} is a wagging motion mainly affecting the hydrogens on terminal atoms. The rotational constants derived for these, as well as the combination band $2\nu_{36}$, are detailed in Table 4. Short descriptions of the motions involved for the vibrations of valinol can be found in Appendix D. In total, the number of assigned vibrational states for each molecule, by conformer, is: 7 for alaninol 1, $g'G'g$; 1 for alaninol 2; $gG'g$; 3 for valinol 1, $g'Gg'G'$. The experimental rotational constants for the observed vibrational states of alaninol 2, $gG'g$ and valinol 1, $g'Gg'G'$ can be found in Tables D1 and D2. The shifted theoretical rotational constants (see Section 3 for details) are included in the tables, which were gleaned from the anharmonic frequency calculations we performed. A direct application of this work is that detected vibrational states could be used as temperature probes for regions where the ground state conformers are detected, for example in hot core regions. Further, the elimination of lines from vibrationally excited states (and isotopologues), which can occupy many channels in astronomical datasets, is an important step in making complex observational spectra more useful by removing lines from already-known molecules.
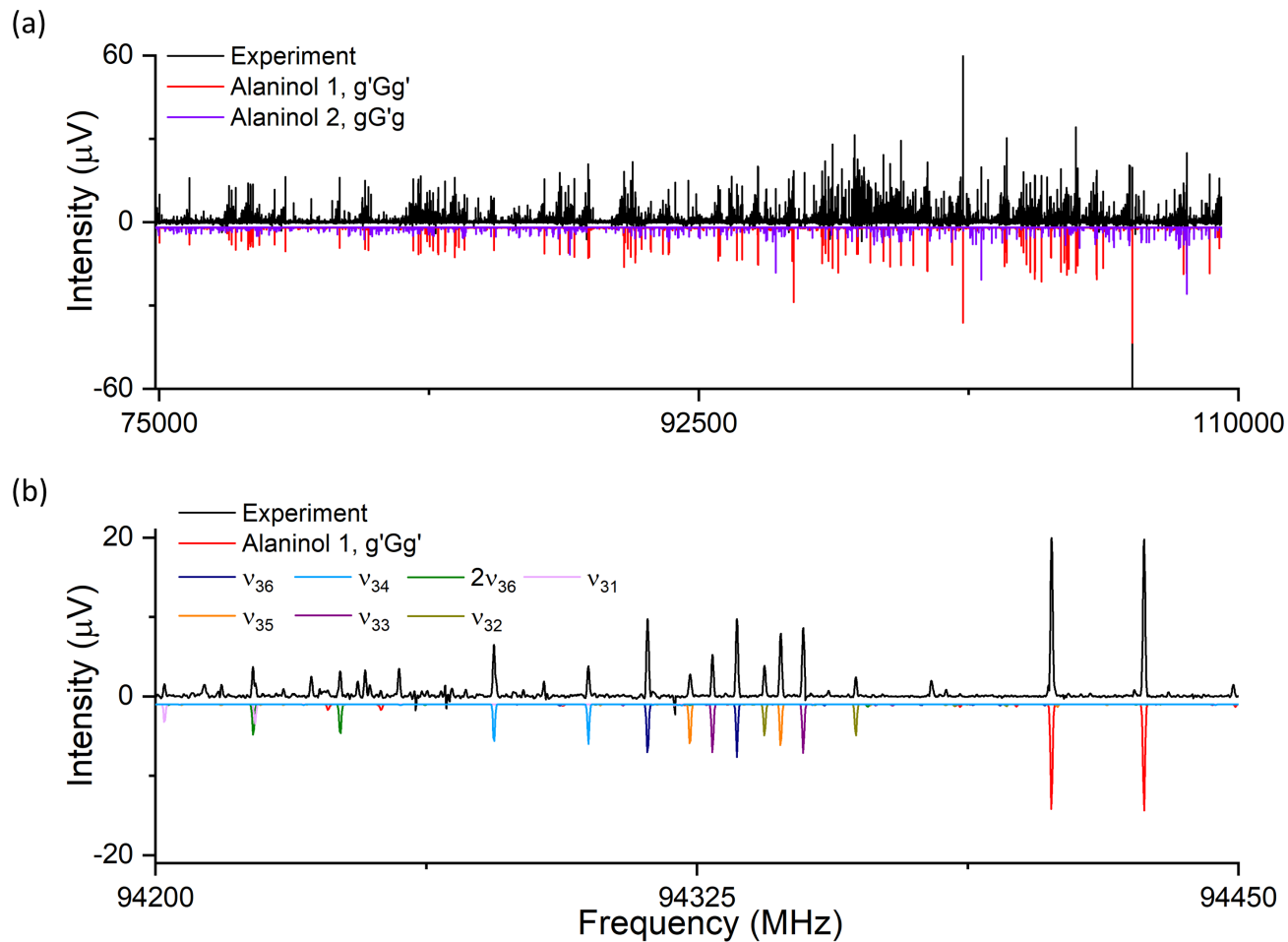
(a)

(b)

Figure 4. (a) High-frequency rotational spectrum of alaninol. The black trace is the experimental spectrum of 500,000 co-added FIDs, and the coloured traces are the simulated spectra based on the fitted rotational constants at 300 K, **which was approximately the temperature of the flow cell.** (b) Zoom-in illustrating the assignment of alaninol 1, $g'Gg'$ and seven fundamental vibrational states of that conformer.

Table 4. The experimental and theoretical rotational constants for the observed vibrational states of the lowest energy conformer of alaninol 1, $g'Gg'$. The theoretical parameters were obtained at the B3LYP-D3(BJ)/aug-cc-pVTZ level of theory and shifted by $\Delta A = 72.3$ MHz, $\Delta B = 52.7$ MHz, and $\Delta C = 31.8$ MHz to account for the differences in the experimental and theoretical rotational constants of the vibronic ground state. The harmonic and anharmonic energies (E^h and E^a respectively) of the vibrational states tabulated are relative to the energy of the alaninol 1, $g'Gg'$ conformer.

	ν_{36}	ν_{35}	ν_{34}	ν_{33}	$2\nu_{36}$	ν_{32}	ν_{31}
E^h / cm^{-1} [kJ mol^{-1}]	146.3[1.8]	228.7[2.7]	257.4[3.1]	266.5[3.2]	292.7[3.5]	365.2[4.4]	451.4[5.4]
E^a / cm^{-1} [kJ mol^{-1}]	151.8[1.8]	219.3[2.6]	251.8[3.0]	262.8[3.1]	306.1[3.7]	363.9[4.4]	457.4[5.5]
A_{theory} / MHz	7907.5	7930.8	7957.6	7965.8	7866.4	7952.8	7940.7
B_{theory} / MHz	3637.5	3637.8	3638.9	3638.7	3634.4	3640.8	3638.0
C_{theory} / MHz	2746.2	2745.4	2742.6	2744.2	2744.6	2745.6	2747.0
A_{exp} / MHz	7907.215(19)	7930.202(22)	7971.968(21)	7948.078(15)	7873.565(20)	7946.558(21)	7922.836(21)
B_{exp} / MHz	3636.4881(14)	3638.1177(18)	3638.3710(15)	3641.2328(12)	3632.5727(16)	3640.4956(15)	3634.6192(19)
C_{exp} / MHz	2745.8447(13)	2745.4712(17)	2742.8480(13)	2744.8387(10)	2743.8372(13)	2745.4025(13)	2741.7037(13)
Δ_J / kHz	0.7308(17)	0.7200(23)	0.7151(19)	0.7222(17)	0.7393(22)	0.7202(22)	0.7209(28)
Δ_{JK} / kHz	3.4823(82)	3.581(12)	3.3912(93)	3.5434(83)	3.500(10)	3.442(13)	3.497(14)
Δ_K / kHz	1.77(51)	2.06(67)	2.49(58)	2.16(44)	2.06(62)	2.60(65)	2.27(69)
δ_J / kHz	0.1766(11)	0.1660(16)	0.1765(12)	0.1738(12)	0.1769(14)	0.1737(14)	0.1788(19)
δ_K / kHz	2.239(31)	2.191(39)	2.539(30)	2.373(26)	2.335(44)	2.294(46)	2.563(39)
No. of lines	78	53	69	68	65	55	51
σ / kHz	24.3	22.5	25.5	18.8	23.4	22.9	22.5

Table 5. The rotational partition functions (Q_{rot}) for alaninol 1, $g'Gg'$ across standard temperatures as implemented in the JPL database (Pickett et al. 1998) and as calculated by SPCAT (Pickett 1991) are tabulated to one decimal place, where $J_{max} = 220$ and $K_{max} = 40$. The vibrational partition function contributions (Q_{vib}) were calculated by considering the theoretical anharmonic energies up to 500 cm^{-1}.

T / K	Q_{rot} [2I+1=1][a]	Q_{rot} [2I+1=3][b]	Q_{vib}
300	94350.6	283051.8	3.899
225	62723.5	188170.5	2.787
150	34638.3	103914.8	1.743
75	12292.0	36876.0	1.090
37.5	4347.6	13042.8	1.003
18.75	1538.7	4616.2	1.000
9.375	545.3	1635.8	1.000
1.5	35.8	107.3	1.000

[a] The 2I+1=1 case does not consider hyperfine splitting.

[b] The 2I+1=3 case considers hyperfine splitting.

Searches for the assigned species in this work in observational datasets require not only accurate rest frequencies, but also information on the relative intensities of the rotational transitions. Partition functions can be used to calculate the absorption coefficients, and hence transition intensities. This information can be further used to calculate column densities of detected species (Mangum & Shirley 2015). The rotational partition functions computed across the standard temperatures implemented in the JPL database (Pickett et al. 1998) are reported in Table 5 for the lowest energy conformer of alaninol 1, $g'Gg'$. Two sets of rotational partition functions are tabulated: one for spin degeneracy equal to 1 (2I+1=1; the case where hyperfine splitting is not considered) and one for spin degeneracy equal to 3 (2I+1=3; the case where hyperfine splitting is considered). A consequence of varying temperature is the change in the intensity distribution of the observed rotational transitions. This can be seen in Figure 5, which shows the simulated spectra for alaninol 1, $g'Gg'$ across a number of temperatures. This plot was made using the rotational partition functions determined for the case where the spin degeneracy is equal to 1. The general distribution of transitions is the same for the case where the spin degeneracy is equal to 3. The rotational partition functions for the other assigned species - the ground state conformers alaninol 2, $gG'g$, valinol 1, $g'Gg'G'$, valinol 2, $g'Gg'G$, valinol 3, $g'Gg'T$, valinol 4, $gG'gG'$, leucinol 1, $g'Gg'Tg$, leucinol 2, $g'Gg'Gg'$, leucinol 3, $gG'gTg'$, the heavy-atom isotopologues, and the vibrationally excited states - can be found in Tables E1-E9. The rotational partition functions were all calculated using the SPCAT program (Pickett 1991), which computes the values by direct summation over the rotational energy levels (Kisiel 2015; Endres et al. 2016). The maximum J and K values considered for the summation calculation for each conformer are detailed in the captions of the relevant tables of rotational partition functions. Further, the contributions of vibrationally excited states to the total partition function have been calculated for all vibronic ground state conformers, and the values are tabulated alongside the rotational partition functions. The vibrational partition function values were determined by considering the anharmonic energies from our calculations, up to the vibrational states with an energy of 500 cm^{-1} with respect to the ground state energy. Combining intensity information, which is provided by these rotational partition function values, with line frequencies is paramount for confirming interstellar detections and calculating column densities in the ISM.

A study such as ours, which covers a large frequency range and includes high-frequency datasets, is essential for facilitating comprehensive interstellar searches. The reason for this is two-fold. Firstly, the large frequency range allows experimental transition frequencies to be directly compared to observational spectra across a number of facilities. For example, data in the 18-26 GHz range could be used for future searches using data from the Next Generation Very Large Array (ngVLA), where nuclear quadrupole coupling could be relevant. Similarly, the line frequencies in the W-band (75-110 GHz) can be directly compared to those from ALMA Band 3 (84-116 GHz), where the hyperfine splitting has
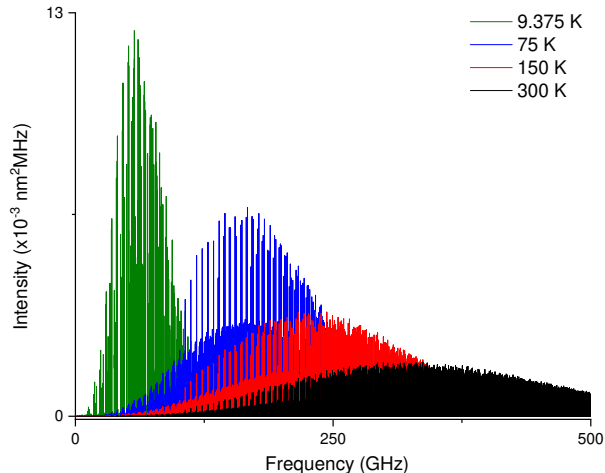
Figure 5. The distributions of rotational transitions of alaninol 1, $g'Gg'$ across four of the standard temperatures implemented in the JPL database; 9.375 K, 75 K, 150 K, and 300 K (Pickett et al. 1998). The maximum frequency simulated here is 500 GHz, and the plot was made for the case where $2I+1=1$. Note that the intensity scale for the prediction at 9.375 K has been halved for a clearer comparison to the other predictions.

little-to-no effect for molecules similar in size to the amino alcohols presented here. This is particularly applicable to the vibrationally excited states we assigned in the room-temperature, high-frequency experiments. Secondly, our high frequency datasets allow us to accurately define centrifugal distortion constants for the molecules we have studied. This can, in the absence of laboratory data higher than 110 GHz, provide more accurate predictions of transition frequencies into the THz regime than if predictions from rotational constants from centimetre-regime data, and thus typically involving low-J transitions, were simply extrapolated. The pitfalls of this were recently highlighted by Martin-Drumel et al. (2019) in their laboratory investigation and interstellar search for vinyl mercaptan. The potential issues presented there are reduced with this present study by providing high-level centrifugal distortion constants for alaninol, valinol, and leucinol.

Appendix F contains information on the machine-readable tables that are available in the electronic supplementary material. The tables contain information about the experimentally assigned transitions for each of the species assigned, as well as predictions for the rotational transitions generated from the experimentally determined rotational, centrifugal distortion, and nuclear quadrupole coupling constants for each assigned species. These predictions are consistent with the format of the `.cat` files produced by the SPCAT program, allowing for ease of application to astrophysical programs, such as CASSIS[2]. This format also matches the format of the CDMS[3] (Müller et al. 2005; Endres et al. 2016) and JPL[4] (Pickett et al. 1998) databases, allowing for the archiving of this information in those databases for both the astrochemistry and molecular spectroscopy communities. It is worthy to note that the tables, in their second columns, also contain predicted line uncertainties calculated by SPCAT. These are predominantly of the order of less than 1 MHz and are therefore useful predictions for both observational searches and further spectroscopic studies. The SPCAT program predicts all lines up to given J and K values, and a handful of lines in the table have larger uncertainties. These transitions are predicted within the range of the provided J and K values, but result from transitions with high lower state energies (generally above 120 cm^{-1}), and are generally low intensity transitions.

The amino alcohols which these predictions pertain to are also attractive targets for interstellar searches due to their relatively high dipole moment components, which are essential for recording laboratory and observational rotational spectra. The components, experimentally determined for alaninol (Ellingsen et al. 1978) and theoretically calculated for valinol and leucinol, are listed in Tables 1-3. The maximum dipole moment components of the molecules are in the region of 3.0 D, which is comparable, for example, to the interstellar molecule *iso*-propyl cyanide (IPC), which has a maximum dipole moment component of μ_a around 4.0 D (Durig & Li 1974). Other examples of similarly complex

---

[2] CASSIS is a software package for the analysis of astronomical spectra developed by IRAP-UPS/CNRS - `http://cassis.irap.omp.eu/`

[3] `http://www.ph1.uni-koeln.de/cdms/`

[4] `http://spec.jpl.nasa.gov/`

molecules have dipole moment components smaller than those of the amino alcohols. For example, aminoacetonitrile has $\mu_a = 2.577(7)$ D (Bogey et al. 1990), and hydroxyacetone has $\mu_a = 2.22(4)$ D and $\mu_b = 2.17(2)$ D (Kattija-Ari & Harmony 1980). This indicates that the effect due to a larger number of heavy atoms in the amino alcohols studied here can be partly compensated by the larger dipole moments. This is highlighted in a comparison of the distribution of rotational transitions for IPC and the lowest energy conformers of alaninol, valinol, and leucinol (Appendix G). The plots show a similar distribution in number and intensity of rotational transitions at 300 K that can be used to confirm the presence of the amino alcohols in the ISM.

6. CONCLUSIONS

This extensive study of the rotational spectra of alaninol, valinol, and leucinol resulted in the observation and assignment of a total of 49 species, including ground state conformers, isotopologues in natural abundance, and low-lying vibrationally excited states. The assignments, comprising of exact transition frequencies between 2-26 and 75-110 GHz and rotational constants up to the quartic centrifugal distortion constants, including the nitrogen nuclear quadrupole coupling constants, are accurately reported here for the first time for the majority of the species observed. The structures of the observed amino alcohols are confirmed with a combination of isotopologue data available in natural abundance and quantum chemical calculations. We see the dominance of the intramolecular hydrogen bond in stabilising the lowest-energy conformers of each molecule, with each exhibiting similar dihedral angles between N(lp)-N-C2-C1, N-C2-C1-O, and C2-C1-O-H.

The present work is paired with our study of the rotational spectrum of isoleucinol, which also details our 18-26 GHz spectrometer for the first time. Together, they provide the astronomical community with the extensive data necessary to search for these astrochemically important molecules. Their detection would establish a new class of compounds observed in the ISM and could point towards areas where their amino acid analogues could be present in the gas phase.

APPENDIX

A. THE NUMBER OF CO-ADDED FIDS PER FREQUENCY RANGE PER MOLECULE

Table A1 is a summary of the number of co-added free induction decays (FIDs) collected per molecule for each frequency range investigated. The experiments were typically performed until there were sufficient signal-to-noise ratios to observe and assign the ^{13}C isotopologues of the lowest energy conformer of each species.

Table A1. A summary of the number of co-added FIDs, in millions, collected per molecule for each frequency range investigated.

Frequency region / GHz	2-8	8-13	13-15.5	15.5-18	18-26	75-110
Alaninol	1.9	1.1	1.0	1.4	2.6	0.5
Valinol	5.6	1.4	1.0	2.3	2.0	0.5
Leucinol	1.0	1.2	1.0	3.0	2.1	0.5

B. NOMENCLATURE

We introduce here the naming system used to refer to the various conformers of alaninol, valinol, and leucinol. Figure 1(a) in Section 1 contains the Lewis structures with carbon atom labels. Each structure is named with a string of letters, for example alaninol 1 is named $g'Gg'$, whereby each letter denotes the magnitude of a defined dihedral angle. In general, the names take the form aBcDe, where the letters refer to the following combinations: a is the dihedral angle N(lp)-N-C2-C1 (where N(lp) is the lone pair of electrons on the nitrogen atom), B is the N-C2-C1-O dihedral angle, and c refers to the C2-C1-O-H dihedral angle (Ellingsen et al. 1978; Fausto et al. 2000). The symbols D and e take different meanings depending on the molecule being considered. D is the C1-C2-C3-H dihedral angle in valinol. In leucinol, D is the C1-C2-C3-C4 dihedral angle, and e is the C2-C3-C4-H dihedral angle. The letter used and the dihedral angle sizes they denote are: g/G for a dihedral angle close to 60° (a *gauche* configuration), g'/G' for a dihedral angle close to -60° (a *gauche* configuration), t/T for a dihedral angle close to 180° (noted as a *trans* configuration in Ellingsen et al. (1978) and Fausto et al. (2000), though commonly also referred to as an *anti* configuration).

C. ANALYSIS OF OBSERVED ISOTOPOLOGUES OF ALANINOL, VALINOL, AND LEUCINOL

The experimental rotational constants for the observed isotopologues of alaninol, valinol, and leucinol are tabulated in Tables C1-C5. Values contained within square brackets were kept fixed to the values of the parent species.

Table C1. The experimental rotational constants for the observed isotopologues of alaninol 1, $g'Gg'$.

	$^{13}\text{C}(1)$	$^{13}\text{C}(2)$	$^{13}\text{C}(3)$	^{15}N	^{18}O
A / MHz	7888.420(50)	7935.239(52)	7876.899(49)	7715.121(56)	7944.579(73)
B / MHz	3557.6341(15)	3631.3380(15)	3626.2698(14)	3635.4848(19)	3461.2597(19)
C / MHz	2693.2494(13)	2744.2287(13)	2732.7080(13)	2716.7871(16)	2644.4232(20)
Δ_J / kHz	[0.72345]	[0.72345]	[0.72345]	[0.72345]	[0.72345]
Δ_{JK} / kHz	[3.4438]	[3.4438]	[3.4438]	[3.4438]	[3.4438]
Δ_K / kHz	[2.024]	[2.024]	[2.024]	[2.024]	[2.024]
δ_J / kHz	[0.17391]	[0.17391]	[0.17391]	[0.17391]	[0.17391]
δ_K / kHz	[2.321]	[2.321]	[2.321]	[2.321]	[2.321]
χ_{aa} / MHz	$-3.723(9)$	$-3.671(9)$	$-3.646(8)$	–	$-3.677(15)$
χ_{bb}-χ_{cc} / MHz	$-0.0560(224)$	$-0.1080(284)$	$-0.1600(236)$	–	$-0.0720(376)$
No. of lines	44	43	44	14	38
σ / kHz	13.8	14.1	13.8	9.4	18.5
J_{max}, K_{max}	4, 4	4, 4	4, 4	4, 4	4, 4

Table C2. The experimental rotational constants for the observed isotopologues of alaninol 2, $gG'g$.

	^{13}C(1)	^{13}C(2)	^{13}C(3)	^{15}N
A / MHz	6348.5973(39)	6442.0197(19)	6421.5158(19)	6309.604(66)
B / MHz	4095.5493(32)	4124.3613(17)	4100.6636(16)	4116.8509(40)
C / MHz	3277.8513(27)	3328.5900(14)	3317.8295(14)	3289.5738(46)
Δ_J / kHz	[1.6343]	[1.6343]	[1.6343]	[1.6343]
Δ_{JK} / kHz	[4.940]	[4.940]	[4.940]	[4.940]
Δ_K / kHz	[−3.701]	[−3.701]	[−3.701]	[−3.701]
δ_J / kHz	[0.24994]	[0.24994]	[0.24994]	[0.24994]
δ_K / kHz	[1.115]	[1.115]	[1.115]	[1.115]
χ_{aa} / MHz	−0.685(20)	−0.705(14)	−0.649(13)	–
χ_{bb}-χ_{cc} / MHz	4.068(72)	4.0384(268)	4.0880(260)	–
No. of lines	21	37	32	5
σ / kHz	20.3	17.4	15.3	3.6
J_{max}, K_{max}	4, 4	3, 3	3, 3	3, 3

Table C3. The experimental rotational constants for the observed isotopologues of valinol 1, $g'Gg'G'$.

	^{13}C(1)	^{13}C(2)	^{13}C(3)	^{13}C(4)	^{13}C(5)	^{15}N	^{18}O
A / MHz	4020.1232(14)	4020.4398(18)	4004.2223(11)	3948.5415(15)	3999.9141(14)	3946.0314(33)	4013.470(74)
B / MHz	1692.8142(46)	1700.92434(56)	1691.58057(49)	1686.74869(48)	1672.71042(54)	1698.5943(10)	1629.6483(14)
C / MHz	1279.64920(35)	1283.99785(42)	1277.09091(38)	1268.26992(38)	1265.72637(36)	1274.83000(51)	1242.5404(12)
Δ_J / kHz	[0.108023]	[0.108023]	[0.108023]	[0.108023]	[0.108023]	[0.108023]	[0.108023]
Δ_{JK} / kHz	[0.18277]	[0.18277]	[0.18277]	[0.18277]	[0.18277]	[0.18277]	[0.18277]
δ_J / kHz	[0.026377]	[0.026377]	[0.026377]	[0.026377]	[0.026377]	[0.026377]	[0.026377]
χ_{aa} / MHz	$-4.157(10)$	$-4.200(17)$	$-4.178(10)$	$-4.189(15)$	$-1.391(9)$	$-$	$-4.213(31)$
χ_{bb}-χ_{cc} / MHz	0.7020(276)	0.668(60)	0.6668(352)	0.696(44)	0.7236(304)	$-$	0.092(392)
No. of lines	69	55	56	71	58	24	19
σ / kHz	13.7	16.8	12.6	15.6	13.1	14.6	13.1
J_{max}, K_{max}	9, 9	9, 9	9, 9	9, 9	9, 9	9, 9	9, 9

Table C4. The experimental rotational constants for the observed isotopologues of valinol 2, $g'Gg'G$.

	$^{13}C(1)$	$^{13}C(2)$	$^{13}C(3)$	$^{13}C(4)$	$^{13}C(5)$	^{15}N
A / MHz	4217.25(26)	4230.96(16)	4227.82(18)	4203.53(14)	4165.46(23)	4161.13(46)
B / MHz	1537.6160(10)	1546.15373(94)	1539.5664(10)	1521.8131(10)	1532.9518(10)	1541.7806(52)
C / MHz	1404.8932(10)	1413.57389(91)	1408.5188(10)	1392.5804(10)	1398.6118(10)	1408.0969(39)
Δ_J / kHz	[0.22047]	[0.22047]	[0.22047]	[0.22047]	[0.22047]	[0.22047]
Δ_{JK} / kHz	[0.12889]	[0.12889]	[0.12889]	[0.12889]	[0.12889]	[0.12889]
Δ_K / kHz	[1.039662972]	[1.039662972]	[1.039662972]	[1.039662972]	[1.039662972]	[1.039662972]
δ_J / kHz	[0.043245]	[0.043245]	[0.043245]	[0.043245]	[0.043245]	[0.043245]
δ_K / kHz	[4.825]	[4.825]	[4.825]	[4.825]	[4.825]	[4.825]
χ_{aa} / MHz	[-3.9918]	[-3.9918]	[-3.9918]	[-3.9918]	[-3.9918]	
χ_{bb}-χ_{cc} / MHz	[-0.6612]	[-0.6612]	[-0.6612]	[-0.6612]	[-0.6612]	
No. of lines	17	20	13	24	14	7
σ / kHz	13.1	11.4	12.0	12.4	12.0	17.2
J_{max}, K_{max}	8, 8	8, 8	8, 8	9, 9	8, 8	8, 8

Table C5. The experimental rotational constants for the observed isotopologues of leucinol 1, $g'Gg'Tg$.

	^{13}C(1)	^{13}C(2)	^{13}C(3)	^{13}C(4)	^{13}C(5)	^{13}C(6)	^{15}N
A / MHz	4025.64(40)	4046.97(36)	4032.59(38)	4046.55(44)	4022.16(48)	3984.01(43)	3980.24(49)
B / MHz	898.26547(49)	903.73248(43)	904.24474(46)	899.37101(47)	890.18423(44)	896.39878(41)	900.95139(47)
C / MHz	870.06898(50)	875.96767(42)	875.77149(45)	871.91906(43)	862.41534(44)	868.61992(40)	873.73532(49)
Δ_J / kHz	0.07430(98)	0.06707(84)	0.07240(90)	0.07210(88)	0.06907(87)	0.07393(78)	0.0717(10)
Δ_{JK} / kHz	0.418(14)	[0.4674]	0.421(21)	0.452(17)	0.524(26)	0.408(11)	0.390(19)
Δ_K / kHz	[1.198]	[1.198]	[1.198]	[1.198]	[1.198]	[1.198]	[1.198]
δ_J / kHz	[0.01315]	[0.01315]	[0.01315]	[0.01315]	[0.01315]	[0.01315]	[0.01315]
δ_K / kHz	[7.583]	[7.583]	[7.583]	[7.583]	[7.583]	[7.583]	[7.583]
χ_{aa} / MHz	[−3.8315]	[−3.8315]	[−3.8315]	[−3.8315]	[−3.8315]	[−3.8315]	−
χ_{bb}-χ_{cc} / MHz	[−1.0472]	[−1.0472]	[−1.0472]	[−1.0472]	[−1.0472]	[−1.0472]	−
No. of lines	64	48	60	57	54	57	35
σ / kHz	15.7	10.7	13.5	13.3	13.4	11.3	11.0
J_{max}, K_{max}	14, 14	14, 14	14, 14	14, 13	14, 14	14, 13	14, 13

d. Vibrationally excited states of alaninol, valinol, and leucinol

The motions of the fundamental vibrational modes of alaninol 1, $g'Gg'$ are described in Section 5. The relative energies of the fundamental modes, as well as a depiction of the main motions, are shown in Figure D1. The rotational constants of the assigned vibrationally excited state of alaninol 2, $gG'g$ are provided in Table D1.
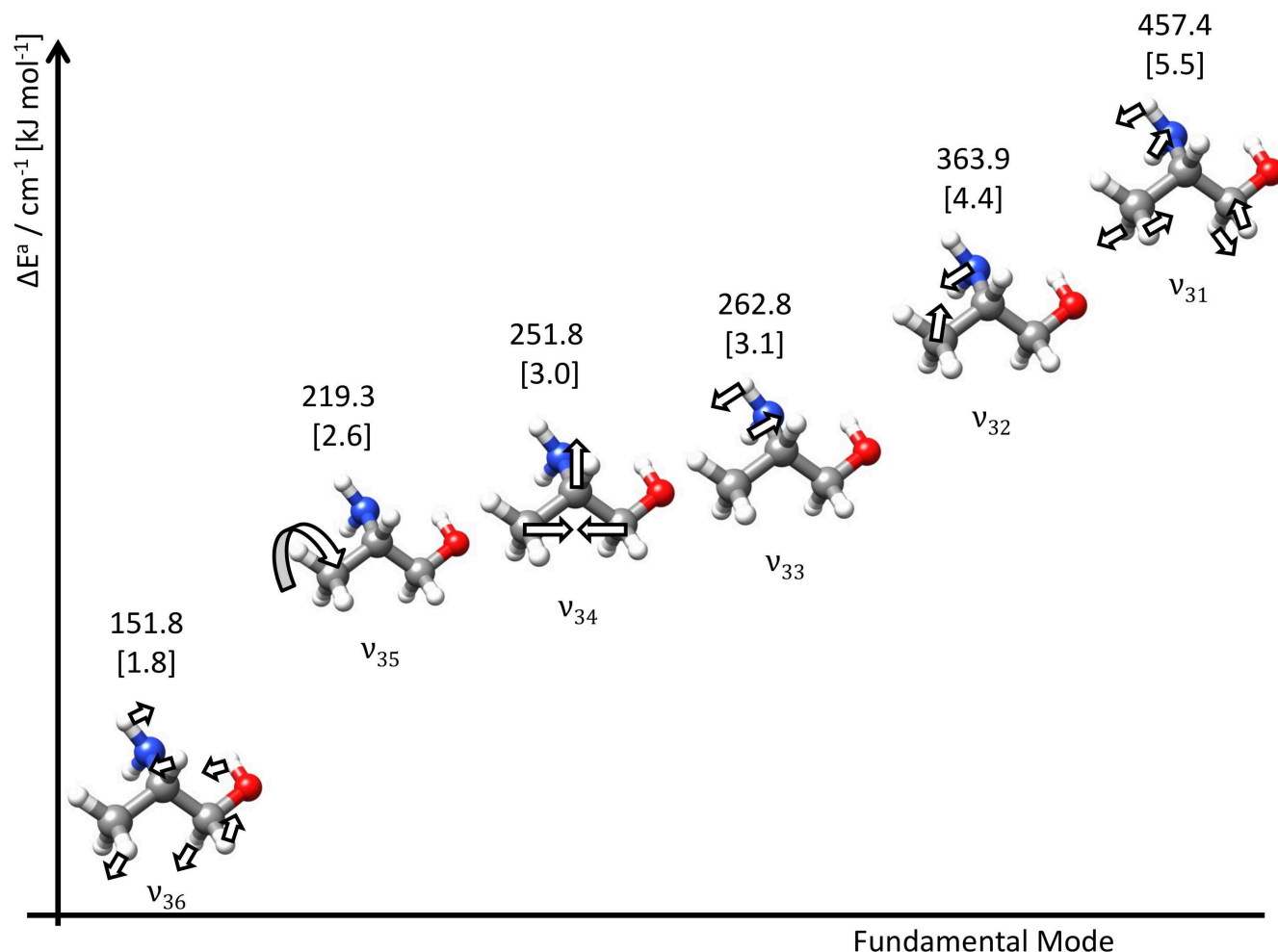

Figure D1. A summary of the assigned fundamental vibrations of alaninol 1, $g'Gg'$. The predominant motion for each mode is indicated by the arrows; a description can be found in the main text. The anharmonic energies presented are those calculated at the B3LYP-D3(BJ)/aug-cc-pVTZ level of theory.

The rotational spectra of three fundamental vibrational modes of valinol 1, $g'Gg'G'$ were assigned in this work. The rotational constants for these states are shown in Table D2. The ν_{54} fundamental mode of valinol 1, $g'Gg'G'$ is a carbon backbone twist. The ν_{53} mode is an asymmetric rocking motion centred on the C1 nucleus. The third state is the overtone of ν_{54}.

The vibrational modes and their associated energies, as obtained from the anharmonic frequency calculations, are presented in Tables D3-D11. The calculations were all performed at the B3LYP-D3(BJ)/aug-cc-pVTZ level of theory; see main text (Section 3) for details. The modes up to 500 cm^{-1} (based on anharmonic energies) are included, and their harmonic (E^h) and anharmonic (E^a) energies are listed to one decimal place.

Table D1. The experimental and theoretical rotational constants for the observed vibrational state of alaninol 2, $gG'g$. The theoretical parameters were obtained at the B3LYP-D3(BJ)/aug-cc-pVTZ level of theory and shifted by the following values to account for the differences in the experimental and theoretical rotational constants of the vibronic ground state: $\Delta A = 35.6$ MHz, $\Delta B = 67.8$ MHz, $\Delta C = 57.9$ MHz. The harmonic and anharmonic energies (E^h and E^a respectively) of the vibrational states are relative to the energy of the alaninol 2, $gG'g$ conformer.

	ν_{36}	
E^h / cm^{-1} [kJ mol^{-1}]	141.4 [1.7]	
E^a / cm^{-1} [kJ mol^{-1}]	139.1 [1.7]	
	This work	Theory
A / MHz	6468.737(31)	6469.0
B / MHz	4138.1980(31)	4136.8
C / MHz	3323.3733(34)	3322.2
Δ_J / kHz	1.6329(51)	
Δ_{JK} / kHz	5.433(29)	
Δ_K / kHz	$-4.28(72)$	
δ_J / kHz	0.2583(34)	
δ_K / kHz	1.333(84)	
No. of lines	46	
σ / kHz	28.5	

Table D2. The experimental and theoretical rotational constants for the observed vibrational states of valinol 1, $g'Gg'G'$. The theoretical parameters were obtained at the B3LYP-D3(BJ)/aug-cc-pVTZ level of theory and shifted by the following values to account for the differences in the experimental and theoretical rotational constants of the vibronic ground state: $\Delta A = 31.0$ MHz, $\Delta B = 18.0$ MHz, $\Delta C = 14.5$ MHz. The harmonic and anharmonic energies (E^h and E^a respectively) of the vibrational states are relative to the energy of the valinol 1, $g'Gg'G'$ conformer. Distortion constants contained within square brackets were kept fixed to the values of the parent species.

	ν_{54}		ν_{53}		$2\nu_{54}$	
E^h / cm^{-1} [kJ mol^{-1}]	74.1 [0.9]		124.3 [1.5]		148.2 [1.8]	
E^a / cm^{-1} [kJ mol^{-1}]	69.7 [0.8]		117.7 [1.4]		139.3 [1.7]	
	This work	Theory	This work	Theory	This work	Theory
A / MHz	4020.001(11)	4019.3	4017.841(12)	4008.5	4009.515(11)	4015.1
B / MHz	1697.89013(67)	1698.1	1694.6255(21)	1702.2	1694.6859(12)	1694.9
C / MHz	1284.60788(48)	1284.8	1285.09357(59)	1284.8	1285.22224(98)	1285.3
Δ_J / kHz	0.10835(25)		0.10933(61)		0.11503(28)	
Δ_{JK} / kHz	0.1909(11)		0.2163(16)		0.15858(80)	
Δ_K / kHz	0.738(78)		[0.724]		[0.724]	
δ_J / kHz	0.02641(13)		0.02709(36)		0.02221(23)	
δ_K / kHz	0.2643(26)		[0.2496]		[0.2496]	
No. of lines	100		31		34	
σ / kHz	25.9		25.0		27.6	

Table D3. Vibrationally excited states of alaninol 1, $g'Gg'$, that reside under 500 cm^{-1} in energy relative to the ground state.

Vibrational mode	E^h / cm^{-1}	E^a / cm^{-1}
ν_{36}	146.3	151.8
ν_{35}	228.7	219.3
ν_{34}	257.4	251.8
ν_{33}	266.5	262.8
$2\nu_{36}$	292.7	306.1
ν_{32}	365.2	363.9
$\nu_{36} + \nu_{35}$	375.0	375.0
$\nu_{36} + \nu_{34}$	403.7	400.9
$\nu_{36} + \nu_{33}$	412.9	413.2
$2\nu_{35}$	457.4	425.9
ν_{31}	451.4	457.4
$\nu_{35} + \nu_{34}$	486.1	470.2
$\nu_{35} + \nu_{33}$	495.2	479.6
ν_{29}	550.0	493.8
$2\nu_{34}$	514.7	496.6

Table D4. Vibrationally excited states of alaninol 2, $gG'g$, that reside under 500 cm^{-1} in energy relative to the ground state.

Vibrational mode	E^h / cm^{-1}	E^a / cm^{-1}
ν_{36}	141.4	139.1
ν_{35}	214.7	208.2
ν_{34}	259.4	248.3
ν_{33}	283.2	265.2
$2\nu_{36}$	282.8	282.1
$\nu_{36} + \nu_{35}$	356.0	346.7
ν_{32}	375.6	373.8
$\nu_{36} + \nu_{34}$	400.8	383.7
ν_{31}	411.2	406.0
$\nu_{36} + \nu_{33}$	424.5	406.6
$2\nu_{35}$	429.3	408.4
$\nu_{35} + \nu_{34}$	474.1	458.1
ν_{30}	529.9	461.5
$\nu_{35} + \nu_{33}$	497.8	470.5
$2\nu_{34}$	518.8	493.3

Table D5. Vibrationally excited states of valinol 1, $g'Gg'G'$, that reside under 500 cm^{-1} in energy relative to the ground state.

Vibrational mode	E^h / cm^{-1}	E^a / cm^{-1}
ν_{54}	74.1	69.7
ν_{53}	124.3	117.7
$2\nu_{54}$	148.2	139.3
$\nu_{54} + \nu_{53}$	198.4	188.5
ν_{52}	190.4	195.7
ν_{49}	269.2	198.4
ν_{50}	240.7	226.4
$2\nu_{53}$	248.6	236.6
ν_{51}	231.6	240.5
$\nu_{54} + \nu_{49}$	343.4	260.9
$\nu_{54} + \nu_{52}$	264.5	268.9
$\nu_{54} + \nu_{50}$	314.8	294.1
ν_{48}	312.2	299.1
$\nu_{53} + \nu_{49}$	393.5	308.8
$\nu_{54} + \nu_{51}$	305.7	312.3
$\nu_{53} + \nu_{52}$	314.7	314.5
ν_{47}	356.0	338.3
$\nu_{53} + \nu_{50}$	365.0	339.5
$\nu_{53} + \nu_{51}$	355.9	358.8
$\nu_{54} + \nu_{48}$	386.4	368.1
$2\nu_{49}$	538.5	368.5
ν_{46}	375.9	374.1
$\nu_{52} + \nu_{49}$	459.6	392.4
$2\nu_{52}$	380.7	393.3
$\nu_{54} + \nu_{47}$	430.1	406.3
$\nu_{53} + \nu_{48}$	436.5	415.5
ν_{45}	427.7	416.7
$\nu_{52} + \nu_{50}$	431.0	420.4
$\nu_{50} + \nu_{49}$	509.9	426.1
$\nu_{51} + \nu_{49}$	500.8	434.1
$\nu_{52} + \nu_{51}$	422.0	439.7
$2\nu_{50}$	481.3	443.9
$\nu_{54} + \nu_{46}$	450.0	446.0
$\nu_{53} + \nu_{47}$	480.3	454.9
$\nu_{51} + \nu_{50}$	472.3	468.1
ν_{44}	483.8	480.0
$2\nu_{51}$	463.2	480.2
$\nu_{54} + \nu_{45}$	501.8	483.9
$\nu_{49} + \nu_{48}$	581.5	489.6
$\nu_{52} + \nu_{48}$	502.6	493.0
$\nu_{54} + \nu_{46}$	500.2	493.7

ARENAS ET AL.

Table D6. Vibrationally excited states of valinol 2, $g'Gg'G$, that reside under 500 cm^{-1} in energy relative to the ground state.

Vibrational mode	E^h / cm^{-1}	E^a / cm^{-1}
ν_{54}	65.9	87.0
ν_{53}	124.1	123.7
$2\nu_{54}$	131.9	181.1
ν_{52}	201.2	195.2
$\nu_{54} + \nu_{53}$	190.0	219.4
ν_{51}	221.7	224.0
ν_{50}	240.4	231.4
$2\nu_{53}$	248.2	246.8
ν_{49}	269.1	264.0
ν_{48}	290.9	286.7
$\nu_{54} + \nu_{52}$	267.1	288.9
$\nu_{54} + \nu_{51}$	287.6	317.4
$\nu_{54} + \nu_{50}$	306.4	319.1
$\nu_{53} + \nu_{52}$	325.3	323.2
ν_{47}	326.2	324.3
ν_{46}	340.6	339.1
$\nu_{53} + \nu_{51}$	345.8	348.5
$\nu_{54} + \nu_{49}$	335.0	351.9
$\nu_{53} + \nu_{50}$	364.5	356.2
$\nu_{54} + \nu_{48}$	356.8	376.3
$\nu_{53} + \nu_{49}$	393.2	384.5
$2\nu_{52}$	402.4	400.3
ν_{10}	3024.4	402.5
$\nu_{54} + \nu_{47}$	392.1	411.4
$\nu_{53} + \nu_{48}$	415.0	412.8
$\nu_{52} + \nu_{51}$	422.9	423.2
$\nu_{54} + \nu_{46}$	406.6	424.6
$\nu_{52} + \nu_{50}$	441.7	429.2
ν_{45}	447.1	439.2
$\nu_{51} + \nu_{50}$	462.1	447.3
$2\nu_{51}$	443.3	447.9
$\nu_{53} + \nu_{47}$	450.3	449.2
$2\nu_{50}$	480.9	458.0
$\nu_{53} + \nu_{46}$	464.8	463.1
$\nu_{52} + \nu_{49}$	470.3	464.5
ν_{43}	544.4	485.1
ν_{44}	496.7	486.3
$\nu_{52} + \nu_{48}$	492.1	488.7
$\nu_{51} + \nu_{49}$	490.8	489.7
$\nu_{50} + \nu_{49}$	509.5	495.1

Table D7. Vibrationally excited states of valinol 3, $g'Gg'T$, that reside under 500 cm^{-1} in energy relative to the ground state.

Vibrational mode	E^h / cm^{-1}	E^a / cm^{-1}
ν_{54}	74.7	43.0
$2\nu_{54}$	149.4	81.1
ν_{53}	122.3	101.8
$\nu_{54} + \nu_{53}$	197.0	139.4
$2\nu_{53}$	244.6	202.5
ν_{52}	215.5	207.8
ν_{51}	231.5	213.5
ν_{50}	245.5	230.7
$\nu_{54} + \nu_{52}$	290.2	252.5
ν_{49}	263.1	255.3
$\nu_{54} + \nu_{51}$	306.2	255.5
ν_{48}	277.7	256.4
$\nu_{54} + \nu_{50}$	320.2	276.1
$\nu_{54} + \nu_{49}$	337.8	293.5
$\nu_{54} + \nu_{48}$	352.4	295.7
$\nu_{53} + \nu_{52}$	337.8	309.0
$\nu_{53} + \nu_{51}$	353.8	312.2
ν_{47}	321.5	316.7
$\nu_{53} + \nu_{50}$	367.8	331.2
ν_{46}	351.4	348.6
$\nu_{53} + \nu_{49}$	385.4	353.7
$\nu_{53} + \nu_{48}$	400.0	355.4
$\nu_{54} + \nu_{47}$	396.2	360.6
$\nu_{54} + \nu_{46}$	426.2	390.5
$2\nu_{52}$	431.0	414.3
$\nu_{53} + \nu_{47}$	443.8	418.5
$\nu_{52} + \nu_{51}$	447.0	420.2
$2\nu_{51}$	463.0	422.4
$\nu_{51} + \nu_{50}$	477.0	429.8
$\nu_{52} + \nu_{50}$	461.0	435.5
$\nu_{53} + \nu_{46}$	473.7	449.8
$2\nu_{50}$	491.1	456.0
ν_{45}	463.5	459.1
$\nu_{52} + \nu_{49}$	478.6	462.4
$\nu_{52} + \nu_{48}$	493.2	463.3
$\nu_{51} + \nu_{48}$	509.2	468.5
$\nu_{51} + \nu_{49}$	494.6	468.6
ν_{43}	550.7	481.4
ν_{44}	500.0	484.2
$\nu_{50} + \nu_{49}$	508.6	485.4
$\nu_{50} + \nu_{48}$	523.2	486.0

Table D8. Vibrationally excited states of valinol 4, $gG'gG'$, that reside under 500 cm^{-1} in energy relative to the ground state.

Vibrational mode	E^h / cm^{-1}	E^a / cm^{-1}
ν_{54}	47.1	54.9
$2\nu_{54}$	94.2	110.1
ν_{53}	122.2	112.7
$\nu_{54} + \nu_{53}$	169.3	169.1
ν_{52}	197.9	197.7
$2\nu_{53}$	244.3	223.1
ν_{51}	227.3	224.2
ν_{50}	242.7	244.8
$\nu_{54} + \nu_{52}$	245.0	258.8
ν_{49}	274.9	259.4
$\nu_{54} + \nu_{51}$	274.4	281.2
ν_{48}	305.8	297.3
$\nu_{54} + \nu_{50}$	289.8	299.2
$\nu_{53} + \nu_{52}$	320.0	311.4
$\nu_{54} + \nu_{49}$	322.0	323.9
$\nu_{53} + \nu_{51}$	349.4	336.9
$\nu_{53} + \nu_{50}$	364.9	356.8
$\nu_{54} + \nu_{48}$	352.9	358.4
$\nu_{53} + \nu_{49}$	397.1	371.6
ν_{47}	383.4	377.2
ν_{46}	394.4	392.5
$2\nu_{52}$	395.7	398.5
$\nu_{53} + \nu_{48}$	427.9	412.5
ν_{45}	416.9	413.4
$\nu_{52} + \nu_{51}$	425.1	417.7
$\nu_{54} + \nu_{47}$	430.5	430.9
$\nu_{52} + \nu_{50}$	440.5	438.7
$2\nu_{51}$	454.5	444.6
$\nu_{54} + \nu_{46}$	441.5	447.8
ν_{44}	461.6	456.3
$\nu_{52} + \nu_{49}$	472.8	457.1
$\nu_{51} + \nu_{50}$	470.0	466.4
$\nu_{54} + \nu_{45}$	464.0	468.0
ν_{43}	527.6	469.6
$\nu_{51} + \nu_{49}$	502.2	483.5
$2\nu_{50}$	485.4	485.4
$\nu_{53} + \nu_{47}$	505.6	489.0
$\nu_{52} + \nu_{48}$	503.6	494.8
$\nu_{50} + \nu_{49}$	517.6	499.6

Table D9. Vibrationally excited states of leucinol 1, $g'Gg'Tg$, that reside under 500 cm^{-1} in energy relative to the ground state.

Vibrational mode	E^h / cm^{-1}	E^a / cm^{-1}
ν_{63}	48.1	12.8
$2\nu_{63}$	96.1	19.8
ν_{62}	88.0	70.7
$\nu_{63} + \nu_{62}$	136.1	76.2
ν_{61}	135.5	128.6
$\nu_{63} + \nu_{61}$	183.6	137.9
$2\nu_{62}$	176.0	139.3
ν_{60}	157.0	139.4
$\nu_{63} + \nu_{60}$	205.1	143.8
$\nu_{62} + \nu_{61}$	223.5	198.0
$\nu_{62} + \nu_{60}$	245.0	205.8
ν_{59}	226.1	210.5
$\nu_{63} + \nu_{59}$	274.1	221.3
ν_{58}	246.2	229.0
ν_{57}	255.9	235.7
$\nu_{63} + \nu_{57}$	304.0	239.5
$\nu_{63} + \nu_{58}$	294.3	239.8
$2\nu_{61}$	271.1	256.9
$\nu_{61} + \nu_{60}$	292.6	267.8
ν_{56}	281.4	269.7
$2\nu_{60}$	314.0	276.6
$\nu_{63} + \nu_{56}$	329.4	277.3
$\nu_{62} + \nu_{59}$	314.1	279.9
$\nu_{62} + \nu_{58}$	334.2	299.0
$\nu_{62} + \nu_{57}$	343.9	309.0
ν_{55}	315.0	313.0
$\nu_{63} + \nu_{55}$	363.0	325.3
$\nu_{61} + \nu_{59}$	361.6	339.1
$\nu_{62} + \nu_{56}$	369.4	341.4
$\nu_{60} + \nu_{59}$	383.1	349.5
ν_{54}	356.5	356.4
$\nu_{61} + \nu_{58}$	381.8	357.0
$\nu_{61} + \nu_{57}$	391.4	360.2
$\nu_{60} + \nu_{58}$	403.2	366.4
$\nu_{63} + \nu_{54}$	404.6	368.0
$\nu_{60} + \nu_{57}$	412.9	372.3
$\nu_{62} + \nu_{55}$	403.0	383.0
$\nu_{61} + \nu_{56}$	416.9	396.5
$\nu_{60} + \nu_{56}$	438.4	406.9
$2\nu_{59}$	452.1	417.7
ν_{53}	420.4	421.2
ν_{52}	426.1	421.3
$\nu_{62} + \nu_{54}$	444.5	426.9
$\nu_{59} + \nu_{58}$	472.3	430.8
$\nu_{63} + \nu_{52}$	474.1	433.4
$\nu_{63} + \nu_{53}$	468.5	434.5
$\nu_{61} + \nu_{55}$	450.5	441.3
$\nu_{59} + \nu_{57}$	482.0	442.6
$\nu_{60} + \nu_{55}$	472.0	451.8
$2\nu_{58}$	492.4	455.3
$\nu_{58} + \nu_{57}$	502.1	460.0
ν_{51}	467.0	463.2
$2\nu_{57}$	511.8	466.4
$\nu_{63} + \nu_{50}$	596.5	466.4
ν_{50}	548.4	466.9
$\nu_{63} + \nu_{51}$	515.1	473.5
$\nu_{59} + \nu_{56}$	507.4	478.8
$\nu_{61} + \nu_{54}$	492.1	486.0
$\nu_{62} + \nu_{52}$	514.1	491.7
$\nu_{62} + \nu_{53}$	508.4	492.2
$\nu_{60} + \nu_{54}$	513.5	495.1
$\nu_{58} + \nu_{56}$	527.6	495.4

Table D10. Vibrationally excited states of leucinol 2, $g'Gg'Gg'$, that reside under 500 cm^{-1} in energy relative to the ground state.

Vibrational mode	E^h / cm^{-1}	E^a / cm^{-1}
ν_{63}	59.2	22.2
$2\nu_{63}$	118.3	32.7
ν_{62}	98.3	90.2
$\nu_{63} + \nu_{62}$	157.5	111.4
ν_{61}	131.1	123.4
$\nu_{63} + \nu_{61}$	190.2	143.6
ν_{60}	176.6	172.5
$2\nu_{62}$	196.6	180.5
$\nu_{63} + \nu_{60}$	235.8	195.0
ν_{59}	232.0	203.9
$\nu_{62} + \nu_{61}$	229.4	212.2
$\nu_{63} + \nu_{59}$	291.2	219.3
ν_{58}	248.1	221.2
ν_{57}	258.6	224.2
$\nu_{63} + \nu_{58}$	307.2	233.7
$\nu_{63} + \nu_{57}$	317.7	242.9
$2\nu_{61}$	262.1	244.8
$\nu_{62} + \nu_{60}$	274.9	259.3
ν_{56}	275.9	268.5
$\nu_{63} + \nu_{56}$	335.1	285.1
$\nu_{62} + \nu_{59}$	330.3	293.8
$\nu_{61} + \nu_{60}$	307.7	296.5
$\nu_{62} + \nu_{57}$	356.9	311.7
$\nu_{62} + \nu_{58}$	346.4	312.5
ν_{55}	321.7	313.3
$\nu_{61} + \nu_{59}$	363.1	326.4
$\nu_{63} + \nu_{55}$	380.9	333.6
ν_{54}	341.8	336.6
$\nu_{61} + \nu_{58}$	379.1	344.2
$2\nu_{60}$	353.2	344.2
$\nu_{61} + \nu_{57}$	389.6	349.2
$\nu_{62} + \nu_{56}$	374.2	355.0
$\nu_{63} + \nu_{54}$	400.9	360.0
$\nu_{60} + \nu_{59}$	408.6	376.3
$\nu_{61} + \nu_{56}$	407.0	388.6
$\nu_{60} + \nu_{58}$	424.7	393.5
$\nu_{60} + \nu_{57}$	435.2	394.7
$2\nu_{59}$	464.0	400.4
$\nu_{62} + \nu_{55}$	420.0	403.3
$\nu_{59} + \nu_{58}$	480.1	412.9
ν_{53}	420.0	415.9
ν_{52}	435.0	423.7
$\nu_{62} + \nu_{54}$	440.1	426.1
$\nu_{59} + \nu_{57}$	490.6	426.8
$2\nu_{57}$	517.1	427.7
$\nu_{61} + \nu_{55}$	452.8	436.3
$2\nu_{58}$	496.1	436.6
$\nu_{60} + \nu_{56}$	452.5	436.6
$\nu_{63} + \nu_{53}$	479.1	437.6
$\nu_{58} + \nu_{57}$	506.6	443.3
$\nu_{63} + \nu_{52}$	494.2	443.8
$\nu_{61} + \nu_{54}$	472.8	460.0
$\nu_{59} + \nu_{56}$	507.9	464.6
ν_{51}	473.2	474.4
$\nu_{58} + \nu_{56}$	524.0	483.2
$\nu_{60} + \nu_{55}$	498.3	485.7
$\nu_{57} + \nu_{56}$	534.5	486.7
$\nu_{63} + \nu_{51}$	532.4	498.1

Table D11. Vibrationally excited states of leucinol 3, $gG'gTg'$, that reside under 500 cm^{-1} in energy relative to the ground state.

Vibrational mode	E^h / cm^{-1}	E^a / cm^{-1}
ν_{63}	48.4	10.1
$2\nu_{63}$	96.8	13.2
ν_{62}	97.6	92.8
$\nu_{63} + \nu_{62}$	145.9	102.2
ν_{61}	128.6	121.1
$\nu_{63} + \nu_{61}$	177.0	124.8
ν_{60}	176.3	163.6
$\nu_{63} + \nu_{60}$	224.7	172.2
$2\nu_{62}$	195.1	186.2
$\nu_{62} + \nu_{61}$	226.2	214.2
$\nu_{63} + \nu_{56}$	323.2	215.0
ν_{59}	225.4	219.7
$\nu_{63} + \nu_{57}$	309.4	220.4
ν_{56}	274.9	222.7
ν_{57}	261.0	223.1
ν_{58}	241.6	224.1
$\nu_{63} + \nu_{59}$	273.7	229.9
$\nu_{63} + \nu_{58}$	290.0	231.3
$2\nu_{61}$	257.2	239.9
$\nu_{62} + \nu_{60}$	273.9	254.8
$\nu_{61} + \nu_{60}$	304.9	284.0
$\nu_{62} + \nu_{56}$	372.4	312.3
$\nu_{62} + \nu_{59}$	322.9	312.5
$\nu_{62} + \nu_{57}$	358.6	313.5
ν_{55}	320.1	315.8
$\nu_{62} + \nu_{58}$	339.2	316.2
$\nu_{63} + \nu_{55}$	368.5	325.0
$2\nu_{60}$	352.6	325.6
$\nu_{61} + \nu_{56}$	403.5	336.1
$\nu_{61} + \nu_{57}$	389.7	339.4
$\nu_{61} + \nu_{59}$	354.0	341.0
$\nu_{61} + \nu_{58}$	370.2	344.0
ν_{54}	355.4	350.8
$\nu_{63} + \nu_{54}$	403.8	362.3
$\nu_{60} + \nu_{59}$	401.7	382.8
$\nu_{60} + \nu_{56}$	451.2	384.5
$\nu_{60} + \nu_{57}$	437.3	385.5
$\nu_{60} + \nu_{58}$	417.9	387.2
ν_{53}	405.9	407.4
$\nu_{62} + \nu_{55}$	417.7	407.6
$\nu_{63} + \nu_{53}$	454.3	417.9
$\nu_{57} + \nu_{56}$	535.9	427.3
$2\nu_{56}$	549.7	433.2
$2\nu_{57}$	522.1	437.3
$\nu_{61} + \nu_{55}$	448.7	437.9
$\nu_{59} + \nu_{57}$	486.4	437.9
ν_{52}	440.1	439.5
$\nu_{59} + \nu_{58}$	467.0	439.7
$\nu_{58} + \nu_{56}$	450.7	439.8
$\nu_{58} + \nu_{57}$	500.2	440.1
$\nu_{62} + \nu_{54}$	516.5	442.3
$2\nu_{58}$	502.6	442.9
$\nu_{63} + \nu_{52}$	453.0	443.0
$\nu_{63} + \nu_{50}$	483.2	446.7
ν_{50}	488.5	450.7
ν_{51}	579.0	451.3
$\nu_{63} + \nu_{51}$	530.6	451.5
$\nu_{61} + \nu_{54}$	477.5	454.5
$\nu_{60} + \nu_{55}$	525.9	459.3
$\nu_{62} + \nu_{53}$	484.0	473.6
$\nu_{60} + \nu_{54}$	496.4	480.3
$\nu_{61} + \nu_{53}$	503.5	500.3

E. PARTITION FUNCTIONS FOR ASSIGNED SPECIES

This Appendix contains the partition functions for the assigned species in this work. For those species whose fits encompass data across both the 2-26 GHz and 75-110 GHz ranges and, for completeness, the ground state conformers of leucinol, two sets of rotational partition functions are tabulated; one set corresponds to the $2I+1=1$ case (without hyperfine splitting), and one set corresponds to the $2I+1=3$ case (with hyperfine splitting). The values were all calculated using the SPCAT program (Pickett 1991), which performs a direct summation over the rotational energy levels (Kisiel 2015; Endres et al. 2016). The temperatures are the standard temperatures implemented in the JPL database (Pickett et al. 1998) and SPCAT (Pickett 1991). The values of J_{max} and K_{max} considered in the summation calculations are detailed in the relevant table captions. Vibrational partition function contributions are listed alongside all ground state conformers. These values were determined by considering the anharmonic energies of the vibrational states up to 500 cm^{-1} with respect to the ground state energy and are all given to **three decimal places**.

Table E1. Rotational partition functions (Q_{rot}) for the isotopologues of alaninol 1, $g'Gg'$, where $J_{max} = 220$ and $K_{max} = 40$.

T / K	Q_{rot} ^{13}C(1) [2I+1=3]	Q_{rot} ^{13}C(2) [2I+1=3]	Q_{rot} ^{13}C(3) [2I+1=3]	Q_{rot} ^{15}N [2I+1=1]	Q_{rot} ^{18}O [2I+1=3]
300	290093.6	283781.0	285406.4	96069.4	140294.9
225	192917.2	188669.5	189815.0	63955.2	115642.5
150	106568.5	104197.5	104862.5	35363.4	81707.9
75	37822.0	36977.3	37218.1	12556.1	36574.6
37.5	13377.2	13078.6	13163.8	4441.0	13606.7
18.75	4734.4	4628.8	4658.9	1571.8	4826.6
9.375	1677.6	1640.3	1650.9	557.0	1710.2
1.5	110.0	107.6	108.3	36.5	112.1

Table E2. Rotational (Q_{rot}) and vibrational (Q_{vib}) partition functions for alaninol 2, $gG'g$, where $J_{max} = 220$ and $K_{max} = 40$.

T / K	Q_{rot} parent [2I+1=1]	Q_{rot} parent [2I+1=3]	Q_{vib}	Q_{rot} ^{13}C(1) [2I+1=3]	Q_{rot} ^{13}C(2) [2I+1=3]	Q_{rot} ^{13}C(3) [2I+1=3]	Q_{rot} ^{15}N [2I+1=1]
300	86814.4	260443.1	4.082	265983.8	261659.2	263141.7	88464.1
225	58300.5	174901.5	2.932	178787.4	175745.7	176770.5	59483.1
150	32518.4	97555.1	1.829	99821.3	98042.4	98631.4	33222.8
75	11597.7	34793.1	1.111	35622.2	34970.3	35184.0	11858.5
37.5	4102.7	12308.0	1.005	12601.4	12370.7	12446.3	4195.0
18.75	1452.2	4356.6	1.000	4460.3	4378.8	4405.5	1484.9
9.375	514.8	1544.3	1.000	1581.0	1552.1	1561.6	526.3
1.5	33.9	101.6	1.000	104.0	102.2	102.8	34.6

Table E3. Rotational (Q_{rot}) and vibrational (Q_{vib}) partition functions for valinol 1, $g'Gg'G'$, where $J_{max} = 310$ and $K_{max} = 40$.

T / K	Q_{rot} parent [2I+1=1]	Q_{rot} parent [2I+1=3]	Q_{vib}	Q_{rot} ^{13}C(1) [2I+1=3]	Q_{rot} ^{13}C(2) [2I+1=3]	Q_{rot} ^{13}C(3) [2I+1=3]	Q_{rot} ^{13}C(4) [2I+1=3]	Q_{rot} ^{13}C(5) [2I+1=3]	Q_{rot} ^{15}N [2I+1=1]	Q_{rot} ^{18}O [2I+1=3]
300	252432.8	757298.3	9.914	760706.5	757585.8	762542.6	769097.7	770495.6	254852.1	787185.8
225	174088.4	522265.2	6.818	524635.4	522481.6	526017.3	530950.9	531533.2	175945.2	542940.1
150	100345.1	301035.2	3.767	302418.1	301175.4	303307.7	306485.0	306512.5	101567.5	313005.2
75	36815.1	110445.2	1.579	110960.6	110504.1	111325.3	112629.6	112511.5	37327.1	114859.6
37.5	13065.4	39196.2	1.087	39380.2	39218.2	39512.2	39984.8	39933.8	13251.7	40764.5
18.75	4621.7	13865.1	1.005	13930.4	13873.1	13977.1	14144.2	14126.1	4687.7	14419.8
9.375	1635.8	4907.3	1.000	4930.3	4910.1	4946.9	5006.0	4999.6	1659.1	5103.4
1.5	105.9	317.7	1.000	319.2	317.9	320.2	324.0	323.6	107.4	330.3

Table E4. Rotational (Q_{rot}) and vibrational (Q_{vib}) partition functions for valinol 2, $g'Gg'G$, where $J_{max} = 310$ and $K_{max} = 40$.

T / K	Q_{rot} parent [2I+1=1]	Q_{rot} parent [2I+1=3]	Q_{vib}	Q_{rot} ^{13}C(1) [2I+1=3]	Q_{rot} ^{13}C(2) [2I+1=3]	Q_{rot} ^{13}C(3) [2I+1=3]	Q_{rot} ^{13}C(4) [2I+1=3]	Q_{rot} ^{13}C(5) [2I+1=3]	Q_{rot} ^{15}N [2I+1=1]
300	249015.5	747046.6	9.296	752640.8	747579.4	750680.5	760570.8	758019.6	251165.8
225	171206.0	513617.9	6.264	517596.2	514023.9	516176.2	523141.5	521654.5	172858.2
150	98274.2	294822.6	3.359	297209.9	295086.7	296338.2	300466.7	299822.8	99359.2
75	35893.5	107680.5	1.418	108592.4	107788.9	108252.1	109810.5	109657.5	36343.0
37.5	12727.4	38182.2	1.046	38507.9	38221.3	38385.9	38941.4	38892.3	12890.0
18.75	4502.0	13506.1	1.001	13621.3	13520.0	13578.1	13774.5	13757.2	4559.6
9.375	1593.5	4780.4	1.000	4821.1	4785.3	4805.8	4875.3	4869.2	1613.8
1.5	103.2	309.6	1.000	312.3	310.0	311.3	315.8	315.4	104.5

Table E5. Rotational (Q_{rot}) and vibrational (Q_{vib}) partition functions for valinol 3, $g'Gg'T$, where $J_{max} = 310$ and $K_{max} = 40$.

T / K	Q_{rot} parent [2I+1=1]	Q_{rot} parent [2I+1=3]	Q_{vib}
300	243028.9	729086.6	10.588
225	168520.4	505561.1	7.490
150	97900.3	293700.8	4.377
75	36253.6	108760.9	1.987
37.5	12892.2	38676.7	1.263
18.75	4560.8	13682.5	1.039
9.375	1614.3	4843.0	1.001
1.5	104.6	313.8	1.000

Table E6. Rotational (Q_{rot}) and vibrational (Q_{vib}) partition functions for valinol 4, $gG'gG'$, where $J_{max} = 310$ and $K_{max} = 40$.

T / K	Q_{rot} parent [2I+1=1]	Q_{rot} parent [2I+1=3]	Q_{vib}
300	224996.6	674989.7	9.614
225	156543.3	469630.0	6.683
150	91391.9	274175.7	3.819
75	34056.4	102169.2	1.721
37.5	12130.3	36391.0	1.152
18.75	4291.5	12874.6	1.015
9.375	1519.1	4557.2	1.000
1.5	98.5	295.5	1.000

Table E7. Rotational (Q_{rot}) and vibrational (Q_{vib}) partition functions for leucinol 1, $g'Gg'Tg$, where $J_{max} = 400$ and $K_{max} = 40$.

T / K	Q_{rot} parent [2I+1=1]	Q_{rot} parent [2I+1=3]	Q_{vib}	Q_{rot} ^{13}C(1) [2I+1=3]	Q_{rot} ^{13}C(2) [2I+1=3]	Q_{rot} ^{13}C(3) [2I+1=3]	Q_{rot} ^{13}C(4) [2I+1=3]	Q_{rot} ^{13}C(5) [2I+1=3]	Q_{rot} ^{13}C(6) [2I+1=3]	Q_{rot} ^{15}N [2I+1=1]
300	418643.6	1255930.9	16.788	1267098.9	1257102.9	1258150.5	1263217.0	1278750.7	1272943.8	422080.7
225	288565.0	865694.9	12.076	873649.0	866529.4	867406.3	870728.9	881736.0	8781863	291206.6
150	166217.5	498652.4	7.295	503441.4	499149.9	499783.4	501561.4	508140.1	506463.9	167958.0
75	60934.3	182802.8	3.488	184643.8	182991.7	183277.2	183873.2	186381.0	185920.3	61662.6
37.5	21618.2	64854.6	2.228	65513.6	64922.6	65027.4	65234.7	66130.5	65978.2	21883.0
18.75	7645.3	22935.8	1.602	23168.8	22960.0	22997.0	23070.2	23386.8	23333.2	7739.0
9.375	2704.8	8114.3	1.189	8196.7	8122.9	8136.0	8161.8	8273.8	8254.9	2737.9
1.5	174.4	523.2	1.000	528.5	523.8	524.6	526.3	533.4	532.2	176.5

Table E8. Rotational (Q_{rot}) and vibrational (Q_{vib}) partition functions for leucinol 2, $g'Gg'Gg'$, where $J_{max} = 400$ and $K_{max} = 40$.

T / K	Q_{rot} parent [2I+1=1]	Q_{rot} parent [2I+1=3]	Q_{vib}
300	390664.9	1171994.6	15.663
225	271684.2	815052.7	11.126
150	158505.8	475517.5	6.502
75	59012.5	177037.4	2.889
37.5	21012.1	63036.3	1.774
18.75	7432.0	22296.0	1.265
9.375	2629.5	7888.5	1.040
1.5	169.7	509.0	1.000

Table E9. Rotational (Q_{rot}) and vibrational (Q_{vib}) partition functions for leucinol 3, $gG'gTg'$, where $J_{max} = 400$ and $K_{max} = 40$.

T / K	Q_{rot} parent [2I+1=1]	Q_{rot} parent [2I+1=3]	Q_{vib}
300	404475.5	1213426.5	16.683
225	281720.5	845161.4	11.902
150	164738.9	494216.5	7.071
75	61519.6	184558.9	3.386
37.5	21923.0	65769.0	2.353
18.75	7754.2	23262.7	1.825
9.375	2743.4	8230.3	1.344
1.5	177.0	530.9	1.000

f. MACHINE-READABLE TABLES FOR ASSIGNMENTS AND PREDICTIONS

Machine-readable tables available online contain the experimentally measured transitions extracted from the `.fit` files produced by the SPFIT program (Tables F1-F49). Note that, where global fits combining low and high frequency data were performed, the transitions have quantum number labelling of the form $J\ K_a\ K_c\ F \leftarrow J'\ K_a'\ K_c'\ F'$. The lines in the W-band do not exhibit hyperfine splitting, making the F quantum number redundant. In these cases, F is set to the same value as J. An example of the machine-readable table is shown in Table F1.

Tables F50-F87 contain the predicted spectra with hyperfine splitting up to 50 GHz at 1.5 K, and Tables F88-F125 contain the predicted spectra with hyperfine splitting up to 50 GHz at 9.375 K. Tables F50-F125 take the format shown in the sample of Table F50. For species that have been assigned in the W-band region, Tables F126-F140 are made available. These files contain the predicted spectra without hyperfine splitting up to 300 GHz at 300 K, and all of these take the form of the example in Table F126. All predictions were produced by using the converged Q_{rot} values (tabulated in Appendix E) at the specified temperatures.

The J_{max} values for each prediction are as follows: alaninol J_{max}=12 for the predictions up to 50 GHz and J_{max}=55 for the predictions up to 300 GHz; valinol J_{max}=20 for the predictions up to 50 GHz and J_{max}=115 for the predictions up to 300 GHz; leucinol J_{max}=30 for the predictions up to 50 GHz and J_{max}=170 for the predictions up to 300 GHz.

Table F1. A sample of the table containing the experimentally measured transitions for alaninol 1, $g'Gg'$.

J	K_a	K_c	F	J'	K'_a	K'_c	F'	observed / MHz	observed-calculated / MHz	blend /MHz
3	1	3	3	3	0	3	2	2610.3327	0.0020	
3	1	3	3	3	0	3	4	2610.7466	−0.0024	
3	1	3	2	3	0	3	2	2611.5936	0.0028	
3	1	3	4	3	0	3	4	2611.6835	0.0010	
3	1	3	3	3	0	3	3	2611.9457	0.0008	

NOTE—Table F1 is published in its entirety in the machine-readable format. A portion is shown here for guidance regarding its form and content.

Table F50. A sample of the table containing the SPCAT prediction for alaninol 1, $g'Gg'$ at 1.5 K up to 50 GHz.

Frequency (MHz)	Uncertainty (MHz)	log[intensity] (nm**2.MHz)	dof	E0 (cm**-1)	gup	MolTag	Code	J	K_a	K_c	F	J'	K_a'	K_c'	F'
7.2332	0	−9.8823	3	5.7462	11	91	304	5	4	1	5	5	4	2	5
7.2337	0	−9.7924	3	5.7462	13	91	304	5	4	1	6	5	4	2	6
7.2338	0	−9.9576	3	5.7462	9	91	304	5	4	1	4	5	4	2	4
8.9937	0.0037	−9.545	3	2.7083	5	91	304	3	3	0	2	3	3	1	3
9.5278	0.0027	−9.4896	3	2.7083	9	91	304	3	3	0	4	3	3	1	3

NOTE—Table F50 is published in its entirety in the machine-readable format. A portion is shown here for guidance regarding its form and content.

Table F126. A sample of the table containing the SPCAT prediction for alaninol 1, $g'Gg'$ at 300 K up to 300 GHz.

Frequency (MHz)	Uncertainty (MHz)	log[intensity] (nm**2.MHz)	dof	E0 (cm**-1)	gup	MolTag	Code	J	K_a	K_c	J'	K'_a	K'_c
223.3978	0.0072	−9.8538	3	72.4782	47	91	303	23	9	14	23	9	15
233.5689	0.0196	−9.8869	3	144.2424	67	91	303	33	12	21	33	12	22
268.7516	0.0058	−9.697	3	55.5031	41	91	303	20	8	12	20	8	13
273.5783	0.0379	−9.8454	3	208.7014	81	91	303	40	14	26	40	14	27
296.4338	0.0187	−9.6619	3	119.8068	61	91	303	30	11	19	30	11	20

NOTE—Table F126 is published in its entirety in the machine-readable format. A portion is shown here for guidance regarding its form and content.

G. COMPARING AMINO ALCOHOLS WITH *ISO*-PROPYL CYANIDE

The figures in this appendix compare the predictions of the lowest energy conformers of alaninol, valinol, and leucinol to that of *iso*-propyl cyanide at 300 K in the 75-110 GHz region. The discussion can be found in the main text.

Figures G1, G2, and G3 show individual comparisons between IPC and the respective amino alcohols in this study. Figure G4 shows a zoom-in of the predictions of all three amino alcohols and IPC around 88250 MHz.
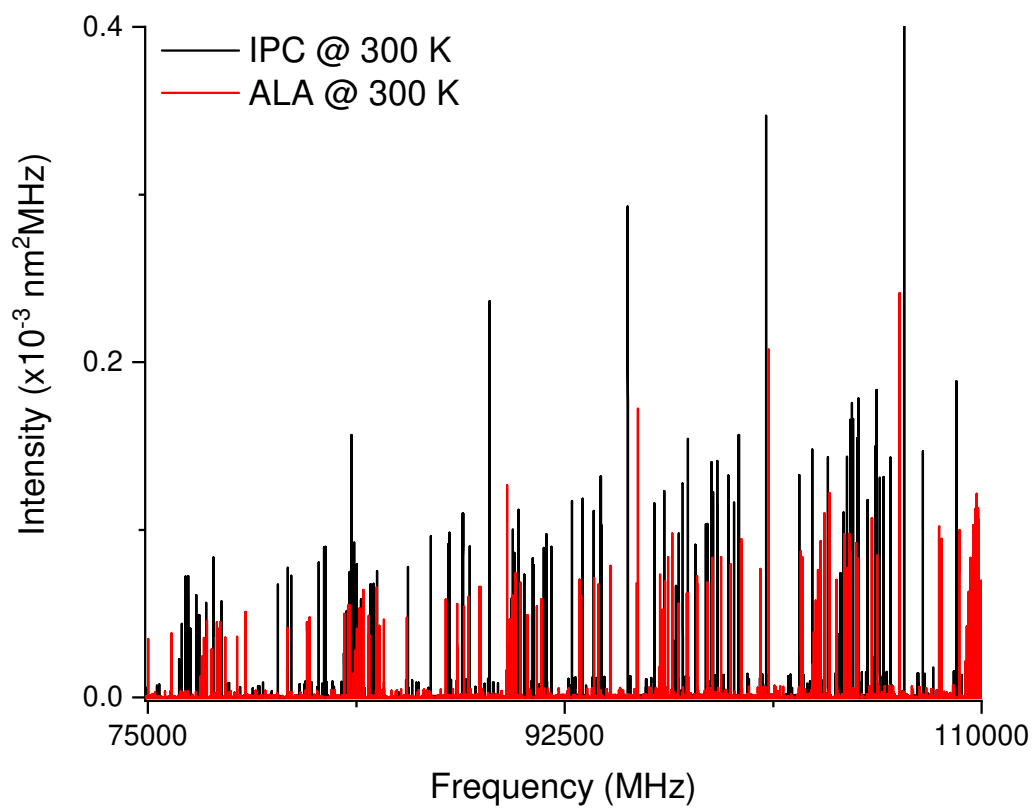
Figure G1. A comparison of distribution of rotational transitions for *iso*-propyl cyanide (IPC) and alaninol 1, $g'Gg'$, at 300 K in the 75-110 GHz frequency region. The similarity in the number and intensity distribution show that alaninol is an attractive target for interstellar searches in areas where, for example, IPC may be found.
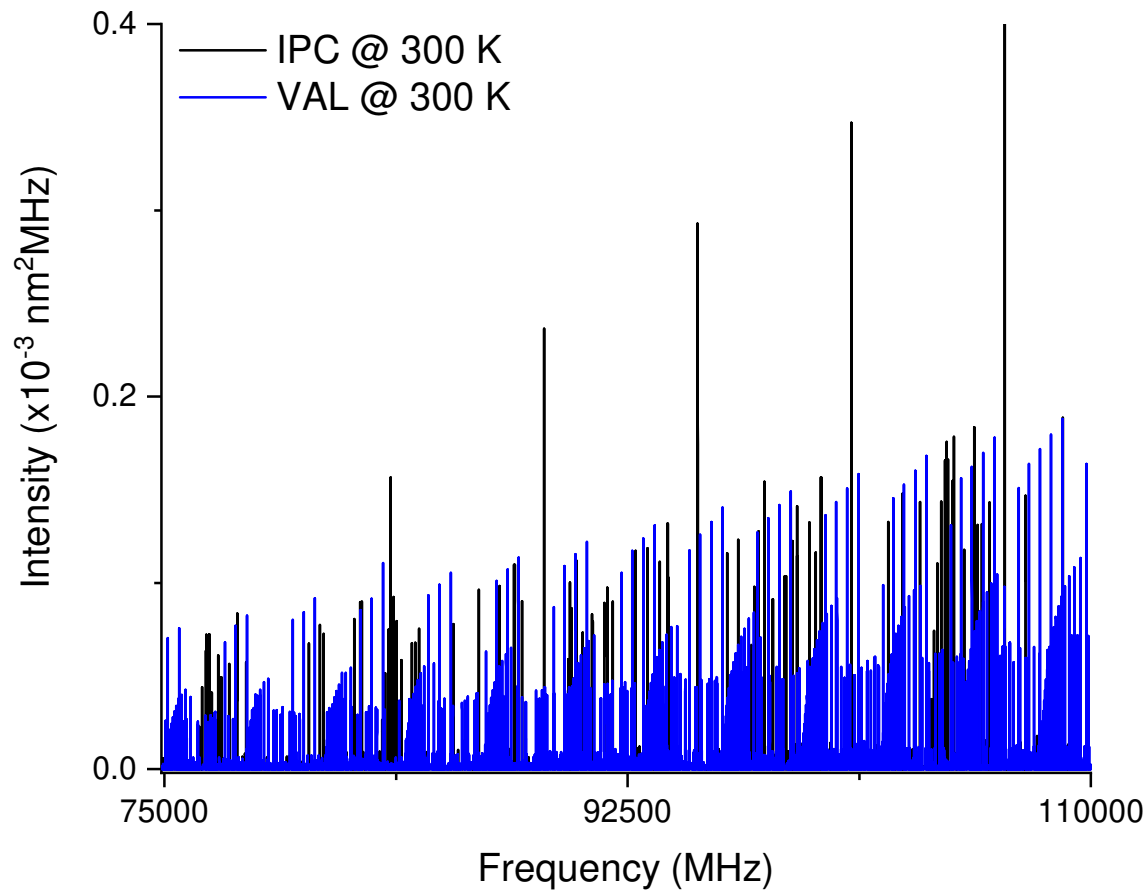
Figure G2. A comparison of distribution of rotational transitions for *iso*-propyl cyanide (IPC) and valinol 1, $g'Gg'G'$, at 300 K in the 75-110 GHz frequency region. The number of rotational transitions available is larger than those available for IPC, and the intensities for the majority of the transitions are of the same order of magnitude.
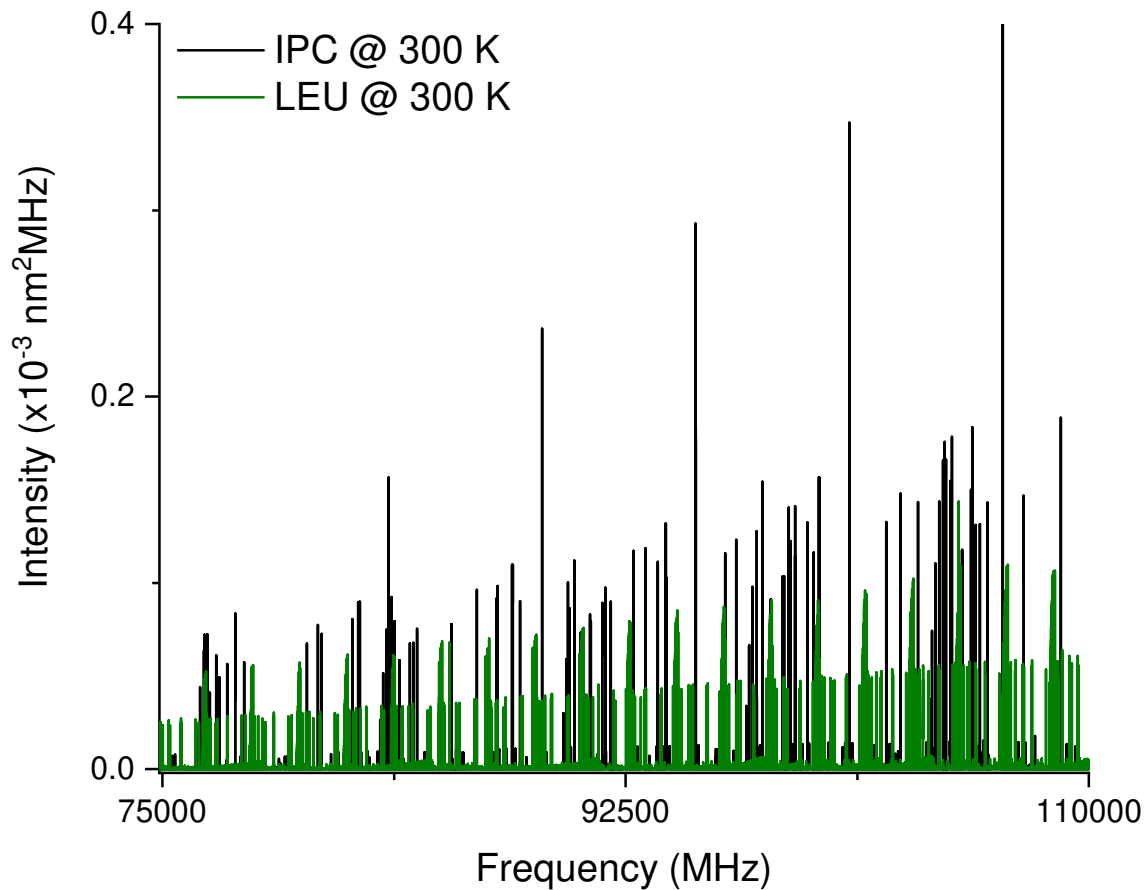
Figure G3. A comparison of distribution of rotational transitions for *iso*-propyl cyanide (IPC) and leucinol 1, $g'Gg'Tg$, at 300 K in the 75-110 GHz frequency region. The more regularly repeating pattern for leucinol shows a greater number of lines in the W-band region when compared to alaninol and valinol, but the intensities are slightly lower.
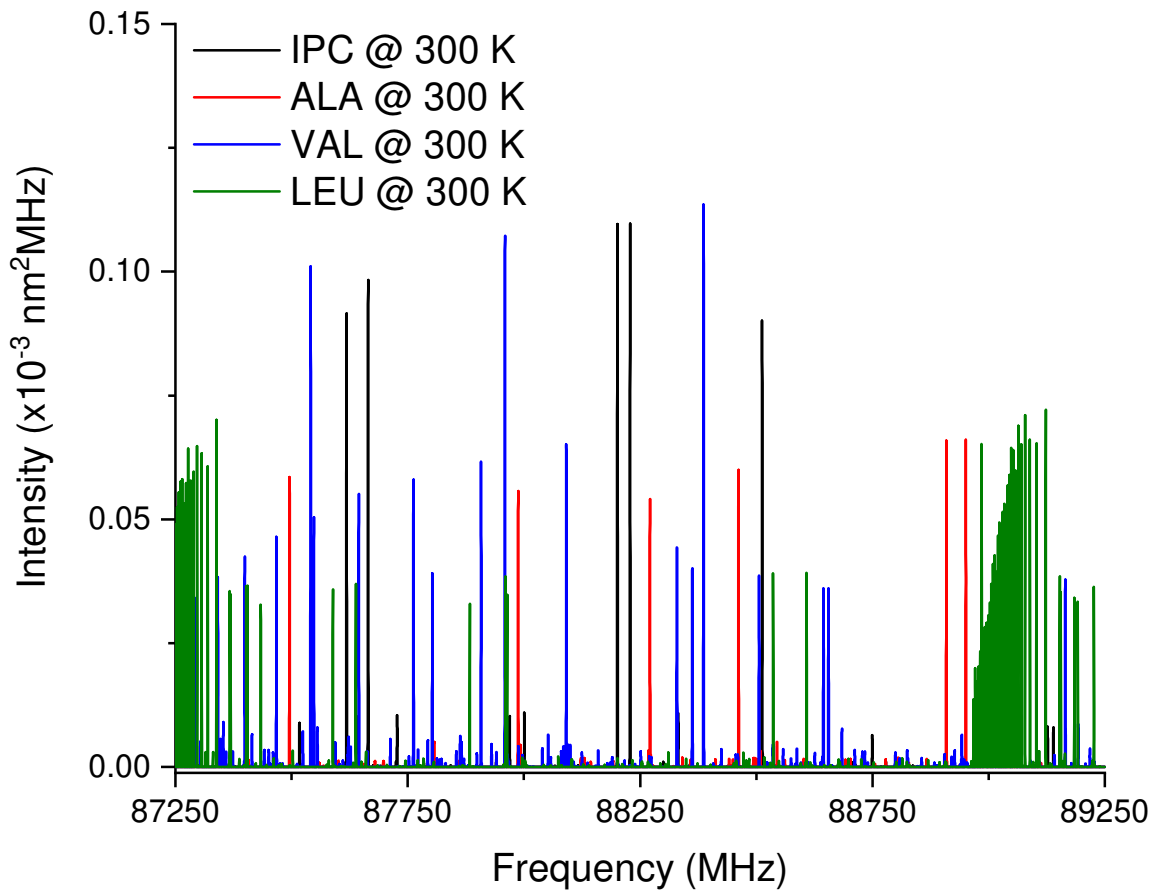
Figure G4. A comparison of distribution of rotational transitions for *iso*-propyl cyanide (IPC) and the lowest energy conformers alaninol 1, $g'Gg'$, valinol 1, $g'Gg'G'$, and leucinol 1, $g'Gg'Tg$, at 300 K around 88250 MHz. The zoom-in shows the distinct and similarly intense lines for the amino alcohols and IPC.

REFERENCES

Altwegg, K., Balsiger, H., Bar-Nun, A., et al. 2016, Science Advances, 2, doi: 10.1126/sciadv.1600285

Arenas, B. E., Gruet, S., Steber, A. L., Giuliano, B. M., & Schnell, M. 2017, Physical Chemistry Chemical Physics, 19, 1751, doi: 10.1039/c6cp06297k

Blanco, S., Lesarri, A., López, J. C., & Alonso, J. L. 2004, Journal of the American Chemical Society, 126, 11675, doi: 10.1021/ja048317c

Bogey, M., Dubus, H., & Guillemin, J. 1990, Journal of Molecular Spectroscopy, 143, 180 , doi: 10.1016/0022-2852(90)90269-V

Christen, D., Coudert, L., Suenram, R., & Lovas, F. 1995, Journal of Molecular Spectroscopy, 172, 57 , doi: 10.1006/jmsp.1995.1155

Cocinero, E. J., Lesarri, A., Grabow, J. U., López, J. C., & Alonso, J. L. 2007, ChemPhysChem, 8, 599, doi: 10.1002/cphc.200600730

Cunningham, M. R., Jones, P. A., Godfrey, P. D., et al. 2007, Monthly Notices of the Royal Astronomical Society, 376, 1201, doi: 10.1111/j.1365-2966.2007.11504.x

Domingos, S. R., Pérez, C., Medcraft, C., Pinacho, P., & Schnell, M. 2016, Physical Chemistry Chemical Physics, 18, 16682, doi: 10.1039/c6cp02876d

Durig, J., & Li, Y. 1974, Journal of Molecular Structure, 21, 289 , doi: 10.1016/0022-2860(74)80052-9

Ellingsen, B. H., Marstokk, K. M., & Møllendal, H. 1978, Journal of Molecular Structure, 48, 9, doi: 10.1016/0022-2860(78)87218-4

Endres, C. P., Schlemmer, S., Schilke, P., Stutzki, J., & Müller, H. S. 2016, Journal of Molecular Spectroscopy, 327, 95, doi: 10.1016/j.jms.2016.03.005

Fatima, M., Pérez, C., Arenas, B. E., Schnell, M., & Steber, A. L. 2020, Physical Chemistry Chemical Physics, Submitted

Fausto, R., Cacela, C., & Duarte, M. L. 2000, Journal of Molecular Structure, 550-551, 365, doi: 10.1016/S0022-2860(00)00396-3

Frisch, M. J., Trucks, G. W., Schlegel, H. B., et al. 2009, Gaussian 09

Furuya, K., Aikawa, Y., Sakai, N., & Yamamoto, S. 2011, The Astrophysical Journal, 731, 38, doi: 10.1088/0004-637x/731/1/38

Giuliano, B. M., Bizzocchi, L., Pietropolli Charmet, A., et al. 2019, Astronomy & Astrophysics, 628, A53, doi: 10.1051/0004-6361/201935769

Hollis, J. M., Lovas, F. J., & Jewell, P. R. 2000, The Astrophysical Journal, 540, L107, doi: 10.1086/312881

Jones, P. A., Cunningham, M. R., Godfrey, P. D., & Cragg, D. M. 2007, Monthly Notices of the Royal Astronomical Society, 374, 579, doi: 10.1111/j.1365-2966.2006.11175.x

Kattija-Ari, M., & Harmony, M. D. 1980, International Journal of Quantum Chemistry, 18, 443, doi: 10.1002/qua.560180845

Kaushik, V., & Woods, R. 1982, Zeitschrift für Physikalische Chemie, 132, 117, doi: 10.1524/zpch.1982.132.1.117

Kisiel, Z. 2015, PROSPE - Programs for Rotational Spectroscopy. http://info.ifpan.edu.pl/Bkisiel/orospe.htm

Kisiel, Z., Pszczółkowski, L., Medvedev, I. R., et al. 2005, Journal of Molecular Spectroscopy, 233, 231, doi: 10.1016/j.jms.2005.07.006

Kraitchman, J. 1953, American Journal of Physics, 21, 17, doi: 10.1119/1.1933338

Kuan, Y., Charnley, S. B., Huang, H., Tseng, W., & Kisiel, Z. 2003, The Astrophysical Journal, 593, 848, doi: 10.1086/375637

Lesarri, A., Cocinero, E. J., López, J. C., & Alonso, J. L. 2004, Angewandte Chemie - International Edition, 43, 605, doi: 10.1002/anie.200352543

Loomis, R. A., Zaleski, D. P., Steber, A. L., et al. 2013, The Astrophysical Journal, 765, L9, doi: 10.1088/2041-8205/765/1/l9

Loru, D., Peña, I., Alonso, J. L., & Eugenia Sanz, M. 2016, Chem. Commun., 52, 3615, doi: 10.1039/C5CC09423B

Mangum, J., & Shirley, Y. 2015, Publications of the Astronomical Society of the Pacific, 127, 266, doi: 10.1086/680323

Martin-Drumel, M.-A., Lee, K. L. K., Belloche, A., et al. 2019, Astronomy & Astrophysics, 623, A167, doi: 10.1051/0004-6361/201935032

McGuire, B. A. 2018, The Astrophysical Journal Supplement Series, 239, 17, doi: 10.3847/1538-4365/aae5d2

McGuire, B. A., Burkhardt, A. M., Kalenskii, S., et al. 2018, Science, 359, 202, doi: 10.1126/science.aao4890

Müller, H. S., Schlöder, F., Stutzki, J., & Winnewisser, G. 2005, Journal of Molecular Structure, 742, 215, doi: 10.1016/j.molstruc.2005.01.027

Neill, J. L., Harris, B. J., Steber, A. L., et al. 2013, Optics Express, 21, 19743, doi: 10.1364/oe.21.019743

Pearson, J. C., Sastry, K. V. L. N., Herbst, E., & De Lucia, F. C. 1997, The Astrophysical Journal, 480, 420, doi: 10.1086/303967

Penn, R. E., & Curl, R. F. 1971, The Journal of Chemical Physics, 55, 651, doi: 10.1063/1.1676133

Pérez, C., Krin, A., Steber, A. L., et al. 2016, The Journal
    of Physical Chemistry Letters, 7, 154,
    doi: 10.1021/acs.jpclett.5b02541

Pickett, H. M. 1991, Journal of Molecular Spectroscopy,
    148, 371, doi: 10.1016/0022-2852(91)90393-O

Pickett, H. M., Poynter, R. L., Cohen, E. A., et al. 1998,
    Journal of Quantitative Spectroscopy and Radiative
    Transfer, 60, 883, doi: 10.1016/S0022-4073(98)00091-0

Schmitz, D., Alvin Shubert, V., Betz, T., & Schnell, M.
    2012, Journal of Molecular Spectroscopy, 280, 77,
    doi: 10.1016/j.jms.2012.08.001

Snyder, L. E., Lovas, F. J., Hollis, J. M., et al. 2005, The
    Astrophysical Journal, 619, 914, doi: 10.1086/426677

Spartan 14. www.wavefun.com

Western, C. M. 2017,
    Journal of Quantitative Spectroscopy and Radiative Transfer,
    186, 221 , doi: 10.1016/j.jqsrt.2016.04.010

Widicus, S., Drouin, B., Dyl, K., & Blake, G. 2003, Journal
    of Molecular Spectroscopy, 217, 278,
    doi: 10.1016/S0022-2852(02)00056-5

Zhang, D., Bocklitz, S., & Zwier, T. S. 2016, The Journal of
    Physical Chemistry A, 120, 55,
    doi: 10.1021/acs.jpca.5b10650

Zuckerman, B., Turner, B. E., Johnson, D. R., et al. 1975,
    The Astrophysical Journal Letters, 196, L99,
    doi: 10.1086/181753